JOURNAL OF QUATERNARY SCIENCE (2022) 1–19 ISSN 0267-8179. DOI: 10.1002/jqs.3452

JQS Journal of Quaternary Science QRA Quaternary Research Association

The dating and correlation of an eastern Mediterranean lake sediment sequence: a 46–4 ka tephrostratigraphy for Ioannina (NW Greece)

AMY M. MCGUIRE,[1]* CHRISTINE S. LANE,[1] KATHERINE H. ROUCOUX,[2] PAUL G. ALBERT[3] and REBECCA KEARNEY[4,5]
[1]Department of Geography, University of Cambridge, Cambridge, UK
[2]School of Geography and Sustainable Development, University of St Andrews, St Andrews, UK
[3]Department of Geography, College of Science, Swansea University, Swansea, UK
[4]Research Laboratory for Archaeology and the History of Art, Oxford, United Kingdom
[5]Section 'Climate Dynamics and Landscape Evolution', GFZ German Research Centre for Geosciences, Telegrafenberg, Potsdam, Germany

Received 10 February 2022; Revised 6 June 2022; Accepted 9 June 2022

ABSTRACT: Terrestrial archives from the Mediterranean have been crucial to expanding our understanding of past environmental variability on a range of timescales. Dating Quaternary sequences in the Mediterranean is, however, often challenging, and age models often have large chronological uncertainties. Tephra deposits can provide crucial age control for detailed environmental reconstructions on sub-centennial timescales. Here, tephra analysis is undertaken for the first time on a sediment core (I-08) from Lake Ioannina, northwest Greece, for the interval spanning 46–4 ka BP. Detailed visible and 'crypto-' tephra analysis identifies deposits associated with explosive volcanism at Italian volcanic sources, including Campi Flegrei, Pantelleria, and the Aeolian Islands. We identify two visible tephra layers, the Campanian Ignimbrite (CI/Y-5; ca. 39.8 ka BP) and Pantelleria Green Tuff (PGT/Y-6; ca. 45.7 ka), as well as the Holocene Vallone del Gabellotto cryptotephra marker (VG/E-1; ca. 8.3 ka BP). Evidence for repeated remobilisation and redeposition of CI tephra material is outlined, and the potential mechanisms and effects of sediment reworking in lake environments are examined. Bayesian modelling, which incorporates the new tephra ages with earlier radiocarbon dates, extends the I-08 core chronology back to ca. 46 ka BP, facilitating direct correlation of the Ioannina sequence to others in the Mediterranean region. © 2022 The Authors *Journal of Quaternary Science* Published by John Wiley & Sons, Ltd.

KEYWORDS: Ioannina; last glacial cycle; Mediterranean; palaeolimnology; tephrochronology

Introduction

Millennial and centennial-scale climate oscillations during the last glacial cycle, such as Dansgaard-Oeschger (D-O) oscillations, were first identified in the Greenland ice core records (e.g. Dansgaard *et al.*, 1982, 1993; Johnsen *et al.*, 1992; Andersen *et al.*, 2004) and, subsequently, in terrestrial and marine sequences throughout the North Atlantic realm and into the Mediterranean (e.g. Bond *et al.*, 1993; Allen *et al.*, 1999; Goñi *et al.*, 2000; Roucoux *et al.*, 2001; Tzedakis *et al.*, 2004). Detailed studies of last glacial sequences have provided important insights into the heterogeneity of climate and environmental responses to abrupt climate change. During the last glacial period oscillations between cold D-O stadial and warm D-O interstadial conditions occurred on timescales of decades or shorter, and are argued to reflect the interplay between internal atmospheric, glacial, and ocean dynamics (Li & Born, 2019; Menviel *et al.*, 2020). Detailed proxy studies with secure chronologies are necessary to examine temporal and spatial variation in the expression of D-O cycles in the Mediterranean region (e.g. Allen *et al.*, 1999).

Developing robust and independently derived chronologies to facilitate accurate inter-site comparisons is a necessary, but complex, task (Lowe *et al.*, 2008; Blaauw *et al.*, 2018). Two main dating approaches are typically used to develop chronologies for long terrestrial sedimentary records from the Mediterranean. Radiocarbon dating is frequently applied to develop chronologies spanning the last 50 ka (e.g. Lawson *et al.*, 2004; Staff *et al.*, 2019). Beyond the 50 ka BP upper dating limit of radiocarbon, pollen records from terrestrial sites can be correlated to their marine equivalents, and, in turn, to the sea surface temperature (SST) and $\delta^{18}O$ records therein, which provide age constraints based on alignment to the Greenland ice cores and orbital parameter, (e.g. Tzedakis, 2002; Tzedakis *et al.*, 2004; Müller *et al.*, 2011; Roucoux *et al.*, 2011). Refining chronologies through correlation approaches, however, inhibits our ability to interrogate relative leads and lags in environmental responses to climate drivers (Blaauw, 2012). Moreover, the large (often millennial-scale) uncertainties inherent in the chronologies to which the records are tuned, such as the layer-counting uncertainty in the Greenland ice core records (e.g. Rasmussen *et al.*, 2014), are rarely factored into tuned age models.

The central and eastern Mediterranean region is home to numerous active and extant volcanic centres and explosive volcanism has produced widespread tephra layers that comprise a well-dated and interconnected tephrostratigraphic framework (see Blockley *et al.*, 2014; Bronk Ramsey *et al.*, 2015; Lowe & Walker, 2015, and references therein), providing scope to test and improve the existing age-depth models of palaeoenvironmental records in the region (e.g. Giaccio *et al.*, 2017; Leicher *et al.*, 2016). Furthermore, tephra markers form time-parallel event horizons (e.g. Lane *et al.*, 2013; Neugebauer *et al.*, 2017) that allow the direct comparison of sequences at and between precise moments in time. By integrating palaeoclimate records from different sites,

*Correspondence: A. M. McGuire, as above.
E-mail: a.mcguire@leeds.ac.uk

tephra studies avoid the often large chronological uncertainties associated with other dating approaches.

Analytical advances over the last two decades have improved our ability to extract, identify, and fingerprint the geochemical composition of glass shards which are not visible within the sedimentary sequence (known as cryptotephra; Blockley *et al.*, 2005; Hayward, 2012). Consequently, tephra deposits can be detected at ever-larger distances from volcanic source regions, increasing the spatial scope of existing tephrostratigraphic frameworks to continental and, in some cases, hemispheric scales (Davies, 2015; van der Bilt *et al.*, 2017).

This paper presents the first tephra study of last glacial and Holocene sediments from the key Mediterranean palaeoecological site of Lake Ioannina, NW Greece. In constructing a last glacial and Holocene tephrostratigraphy for Lake Ioannina we create opportunities for direct correlation of the valuable proxy record of millennial- and centennial-scale change contained therein (see Lawson *et al.*, 2004; Tzedakis *et al.*, 2004; Jones *et al.*, 2013) to other key sites in the central and eastern Mediterranean region. In doing so, we allow for an interrogation of the sequencing of local climate and environmental responses to Dansgaard-Oeschger cycles at the periphery of the North Atlantic climate system.

Study site

Lake Ioannina is located in the interior of the Epirus region of northwest Greece, in the western foothills of the Pindus mountain range (Fig. 1a). The Ioannina basin, ca. 470 m a.s.l., is situated within a tectonic depression bounded by the gently sloping Tomarochoria mountains to the west and the steep-sided Mitsikeli mountain to the east. The growth of the basin has been attributed to karst solution and subsidence (Lawson, 2001, *and references therein*). The lake itself (also known as Lake Pamvotis) has undergone extensive artificial drainage, culminating in 1959 when the northerly Lapsista sub-basin (previous water depth 1–3 m) was converted to agricultural land (Romero *et al.*, 2002). Whilst the 'natural' (pre-drainage) scale of the lake basin is not known, it may have been as large as 20 km (Conispoliatis *et al.*, 1986). The longest retrieved sediment record is core I-284, recovered by the Greek Institute of Geology and Mineral Exploration (IGME), which records continuous sedimentation back >250 ka BP (Tzedakis, 2002; Lawson *et al.*, 2004; Roucoux *et al.*, 2008, 2011).

The present-day lake (Fig. 1b), located near the foot of Mitsikeli mountain in the southeast of the original basin, is 11 km on its longest axis, with a surface area of ca. 23 km^2. The modern lake is shallow, with a maximum water depth of 10 m, and is a closed system with no major fluvial inputs, although ephemeral streams have been identified within the basin (Lawson, 2001). The lake is primarily fed by springs, most notably at the foot of the Mitsikeli Ridge (Fig. 1b; Higgs *et al.*, 1967). Drainage occurs through sinkholes, termed *katavothrai*, located throughout the basin (Higgs *et al.*, 1967).

Previous work at Ioannina has identified millennial-scale expansions and contractions of tree populations which have been linked to climate oscillations recorded in Greenland and throughout the North Atlantic, however, tuned chronologies inhibit interrogation of the timing of these responses relative to other sites in the Central and Eastern Mediterranean (Tzedakis *et al.*, 2004). More recent studies have sought to generate independent, well-resolved age models for the site (e.g. Jones *et al.*, 2013), however, chronological limitations continue to complicate inter-site comparisons. In particular, the hard-water effect, whereby ^{14}C ages are artificially inflated by unquantifiable amounts of old, inert carbon derived from the karstic bedrock (Shotton, 1972), coupled with the absence of terrestrial macrofossils and macrocharcoal, limit the utility of radiocarbon dating at the site. Through integrating the Ioannina site into the wider Mediterranean tephra framework, we seek to open up opportunities for direct correlation, providing new insights into how the relative timing of proxy responses to climate forcing vary spatially.

There is significant potential for locating tephra layers in the Ioannina sediment record. Ioannina lies to the east of several Italian volcanoes which have been active throughout the Quaternary (Fig. 1a), and thus the site is located downwind of these volcanoes assuming the present-day prevailing westerlies were dominant during the last glacial. Widespread tephra layers, found in sedimentary sequences across the Central and Eastern Mediterranean basin, have been generated by eruptions from the Campanian and Roman Volcanic Zones (Tomlinson *et al.*, 2012; Marra *et al.*, 2020), the Aeolian Island volcanoes (Albert *et al.*, 2017), and Pantelleria Island (Jordan *et al.*, 2018). The Aegean Arc volcanoes, e.g., Santorini, Nisyros, Yali and Kos, lie<1, 000 km southeast of Ioannina and were also active during the last glacial and tephra layers have been found in both terrestrial and marine sedimentary archives (e.g. Eastwood *et al.*, 1999; Karkanas *et al.*, 2014; Wulf *et al.*, 2020).

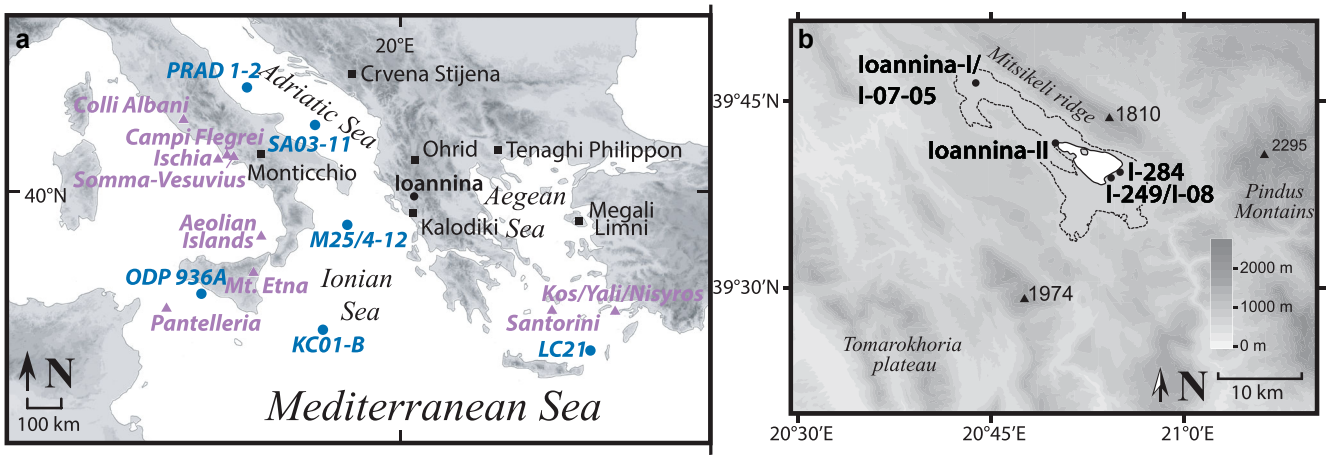

Figure 1. Maps showing (a) the location of the Ioannina site, along with Quaternary terrestrial (black squares) and marine (blue circles) sediment sequences featured in the text, alongside volcanic centres with known last glacial and Holocene activity (purple triangles) and (b) the Ioannina catchment, showing local topography, the present day lake (solid line), the limit of lake sediment deposits (dotted line), and the location of I-08 and earlier core sites. [Color figure can be viewed at wileyonlinelibrary.com]

Methods and materials

Core recovery

The I-08 core site (39°39.0350′N, 20°54.8990′E; Fig. 1b) lies near the earlier I-249 core site (Tzedakis, 1994), towards what would have been the centre of the lake prior to drainage. Core I-08 was recovered in 2008 from a single borehole using a truck-mounted drill, which maintained the vertical integrity of samples, with a core recovery >90%. Cores were stored in steel tubing at temperatures <6°C. Coarse sand dominates between 21.00 and 19.71 m, and the remainder of the sequence consists mainly of carbonate clays and silts.

Jones *et al.* (2013) developed a chronology for the upper 21 m of the I-08 sequence through radiocarbon dating using a novel approach which combined radiocarbon dates from microcharcoal concentrates with dates determined through compound-specific radiocarbon analysis (CSRA). More specifically, Jones *et al.* (2013) measured of the ^{14}C content of long-chain, odd-numbered n-alkanes which originate from epicuticular waxes of terrestrial higher plants, thus circumventing the impact of local lake reservoir effects. Here we build on this chronology through tephra study from 12 m depth (early Holocene) to the base of the core at 37 m, which covers part of the last glacial (coeval with Marine Isotope Stages 3 and 2).

Sediment analyses

Sediment logging was undertaken throughout the I-08 core sequence to detect any visible changes in sedimentology which may reflect changes in the sedimentary regime at the core site. Visible tephra layers were identified on visual inspection of the core, and confirmed using low-powered microscopy to identify volcanic glass shards. Visible tephra deposits were wet-sieved to remove <25 μm particles, allowing the characterisation of glass shard morphology and subsequent geochemical analysis.

Particle size analysis was undertaken to supplement sediment logging on a complex unit between 28 and 32 m depth where multiple changes in grain size were observed. 323 contiguous 1 cm (ca. 1 g) sediment samples were treated with sodium pyrophosphate to deflocculate clays and analysed using a Malvern Mastersizer in the Department of Geography, University of Cambridge.

X-ray fluorescence scanning was used to analyse the chemical composition of I-08 core sediments. Measurements span the entire 38 m sequence, undertaken at 2 mm intervals using the Avaatech core scanner in the Godwin Laboratory for Palaeoclimate Research, Department of Earth Sciences, University of Cambridge.

Cryptotephra extraction and identification

Cryptotephra investigations were carried out in two stages. An initial range-finding investigation analysed contiguous 10 cm long (ca. 5 g) samples of sediment, and was followed by contiguous 1 cm analyses through sections of the core that were identified as containing peaks in tephra glass shard concentrations.

Samples were dried, weighed, and soaked in 3% hydrochloric acid to remove carbonates. For sections of the core where the initial 10 cm samples had glass shard concentrations of >10 000 shards g^{-1}, *Lycopodium* tablets of known concentration were added to subsequent 1 cm (ca. 1 g) samples (Gehrels *et al.*, 2006).

Samples were wet sieved at 25 μm, with the >25 μm remainder density separated using a heavy liquid (sodium polytungstate) solution at 1.95 and 2.55 g cm^{-3} (Blockley *et al.*, 2005). After extraction the 1.95–2.55 g cm^{-3} fraction was sieved again at 25 μm to remove any residues and mounted onto microscope slides using Canada Balsam.

Glass shards were identified at ×400 using a high-powered, polarising optical microscope. In samples where marker spores were added glass shard concentrations were calculated in shards g^{-1} dry weight calculated by multiplying the number of *Lycopodium* spores in the tablet by the ratio of glass shards counted to *Lycopodium* marker spores counted. Peaks in glass shard concentration were identified as potential ash fall layers and assigned depth codes based on the lower bound of the sediment unit containing the peak.

Geochemical analysis of tephra samples

Intervals with distinct peaks in glass shard concentration at 1 cm resolution, identified as containing potential primary airfall deposits, were re-extracted using the above protocols and prepared for geochemical analysis. Low concentration tephra horizons (<500 shards g^{-1}) were concentrated by picking out individual glass shards using a gas chromatography syringe mounted on a micromanipulator (Lane *et al.*, 2014). Both visible and cryptotephra samples were mounted in epoxy resin, then ground and polished to expose flat internal glass shard surfaces for electron microprobe analysis.

Samples from 12 to 20 m depth were analysed for major and minor element concentrations using the JEOL, Freising, Germany-8600 wavelength-dispersive electron microprobe (WDS-EPMA) at the Research Laboratory for Archaeology and History of Art, University of Oxford. A 15 keV accelerating voltage and 6nA beam current were used, along with a defocused (10 μm) beam. Secondary glass standards Atho-G and StHs6/80-G were used as a check on accuracy and precision of the EPMA data. All other samples were analysed using a Cameca, Gennevilliers, France SX100 WDS EPMA at the Department of Earth Sciences, University of Cambridge. Analyses utilised a 15 keV accelerating voltage, a 10 nA beam current, with a 10 μm diameter unfocused beam. Secondary standards KL2-G, T1-G, GOR 128-G, ATHO-G and STHS6/180G (Jochum & Willbold, 2006) were analysed before, between, and after batches of analyses to ensure consistency between sessions.

Trace element analyses used the Agilent 7500es ICP-MS coupled to a Resonetics 193 nm ArF excimer laser-ablation in the Department of Earth Sciences, Royal Holloway, University of London following analytical procedures outlined in Tomlinson *et al.* (2010). The repetition rate was 5 Hz and the count time 40 s on the sample and 40 s on the gas blank to determine the background signal. Blocks of eight sample/shards of glass and one MPI-DING reference glass were bracketed by NIST612 glass calibration standard (GeoREM 11/2006). The internal standard applied was ^{29}Si, as determined by grain-specific EPMA analysis. ATHO-G, StHs6/80-G and GOR128-G were used as secondary standards (Jochum & Willbold, 2006).

Full EPMA, LA-ICP-MS, and associated secondary standard data can be found in Supplementary Information 1.

Age-depth model

The new I-08 age-depth model incorporates new dates imported through the application of tephrochronology alongside previously-published radiocarbon dates (Jones *et al.*, 2013). An updated I-08 age-depth model was constructed using a Bayesian approach implemented in OxCal v4.4 (Bronk Ramsey, 2020), using the IntCal20 calibration curve (Reimer, 2020). The P_Sequence deposition model was used, with a low rigidity ($k = 10$) applied, allowing for

increased uncertainty ranges in the sections of core between dates (Ramsey, 2008; Ramsey & Lee, 2013). A 'general' outlier model, with a 5% prior probability of any individual date being a statistical outlier, was applied (Bronk Ramsey, 2009). See Supplementary Information 2 for radiocarbon dates and OxCal code.

Results

In this section we present the results of both visible and cryptotephra study of the I-08 core, as well as our correlations to published proximal and distal glass shard geochemical data from sites in the Mediterranean region.

Visible tephra deposits

The I-08 core contains two visible tephra deposits. The lower tephra deposit, from 31.93 to 31.92 m depth, henceforth I08T_31.93, forms a clearly defined 1 cm layer in the stratigraphy with an abrupt contact at the base. The much larger upper tephra deposit 29.91 to 30.14 m depth, I08T_30.14, shows some fining towards the surface, however, the base is less clearly delineated as it falls at the end of a core section. Microscopic inspection of sediments within these lighter horizons revealed that they contained a high concentration of volcanic glass shards.

I08T_31.93 - Y-6/Pantelleria Green Tuff

I08T_31.93 is a <1cm thick layer that is visible within the stratigraphy due to its lighter, beige colour compared to the surrounding olive-coloured sediments. The bottom of the I08T_31.93 unit is marked by an abrupt contact with the underlying lake sediments. Tephra glass shards in I08T_31.93 have varied morphologies; primarily they are platy and fluted, with fewer cuspate shapes. Maximum long axis lengths are 110 µm. Tephra glass shards in I08T_31.93 are predominantly light olive in colour under plane polarised light.

The geochemical composition of I08T_31.93 glass shards is predominantly rhyolitic ($n = 20$) with a limited number ($n = 2$) of trachytic shards (Fig. 3a). SiO_2 ranges from 64.2 to 72.5 wt.% and Na_2O (4.1–2.9 wt.%) is generally greater than K_2O (4.1–2.8 wt.%). The rhyolitic glass shards are pantelleritic following a peralkaline classification, where FeO_t (7.1–2.7 wt.%) and Al_2O_3 (7.1–2.6 wt.%) are near equal in their abundance (Fig. 3b). The two trachytic shards have lower FeO_t (6.1–2.5 wt.%) and increased Al_2O_3 (11.1–24.0 wt.%) than the rhyolitic glass shards (Table 1).

The major and minor element composition of I08T_31.93 (Table 1) corresponds in full to the proximal glass compositions of the Pantelleria Green Tuff (PGT; Civetta *et al.*, 1984; Tomlinson *et al.*, 2015), correlated to the Y-6 tephra marker identified in marine sequences from the Ionian Sea (Keller *et al.*, 1978, Table S7). Eruptions from anorogenic volcanism on Pantelleria Island are clearly distinguished from other Mediterranean sources by their high SiO_2 and low Al_2O_3 content (Tomlinson *et al.*, 2015). Whilst other widespread Pantellerian tephra markers have been identified in the Mediterranean, the Green Tuff is easily discriminated on the basis of FeO_t concentrations (Hardiman, 2012). I08T_31.93 FeO_t concentrations (Fig. S1B) closely match both proximal PGT (Tomlinson *et al.*, 2015) and distal Y-6 (Vogel *et al.*, 2010; Tamburrino *et al.*, 2012).

The Pantelleria Green Tuff was produced during a caldera-forming eruption of the Island of Pantelleria in the Sicily channel, dated to 45.7 ± 1.0 ka using the $^{40}Ar/^{39}Ar$ method (Scaillet *et al.*, 2013, Table S7). We incorporate this best age for the Pantelleria Green Tuff eruption into the I-08 age-depth model at 31.93m (Fig. 2).

I08T_30.14 - Y-5/Campanian Ignimbrite

The I08T_30.14 tephra unit (Fig. 2) appears ca. 18 cm thick, however, as 7 cm of material is missing between 30.21 and 30.14 m depth, due to the core extraction process, the true thickness of this tephra deposit is uncertain. As the underlying core section, with its surface at 30.21 m, contains a ca. 5 cm drop-stone of agglomerated ash it is likely that the missing section of the lake sequence was predominantly tephra. Overlying and underlying sediments are generally well compacted clays and silts, less likely to be lost during core extraction than disaggregated, coarse grained tephra. Therefore, it is possible that the thickness of the I08T_30.14 deposit is as much as 25 cm, indicative of an eruption that generated a significant amount of ash-fall and potential secondary thickening from re-deposition at the upper contact.

The I08T_30.14 tephra deposit primarily consists of colourless glass shards with varied morphologies, however, the majority of shards are either platy or fluted. Particle size distributions of tephra glass shards are unimodal, with some evidence of fining upwards through the deposit (Fig. S2).

I08T_30.14 glass shard major and minor element compositions straddle the phonolite-trachyte boundary with SiO_2 ranging from 60.9 to 62.3 wt.% and total alkalis ranging from 13.8 to 14.0 wt.%. Glass compositions are potassium rich (K_2O: 7.1–20.3 wt.%) with lower sodium (Na_2O: 3.01–2.15 wt.%; Table 1), consistent with magma erupted from the Campanian Volcanic Zone (Fig. 3).

I08T_30.14 glass compositions are consistent with glass compositions of the Campanian Ignimbrite (CI) generated from a caldera forming eruption of the Campi Flegrei volcano, Italy, ca. 40 ka BP and correlated to the widely-recognised Y-5 marine tephra in the Mediterranean tephrostratigraphy (Keller *et al.*, 1978). The Campanian Ignimbrite eruption is one of the largest known Quaternary eruptions, with tephra deposits

Table 1. Representative shard-specific normalised major and minor element (WDS-EMPA) glass data for visible tephra units I08T_30.14 and I08T_31.93.

	SiO_2	TiO_2	Al_2O_3	FeO_t	MnO	MgO	CaO	Na_2O	K_2O	P_2O_5	Cl
I08T_30.14											
Average	61.08	0.41	18.45	3.00	0.19	0.41	1.97	5.52	8.02	0.07	0.90
2 s.d.	1.22	0.09	0.55	0.44	0.13	0.32	0.70	2.48	2.01	0.09	0.55
I08T_31.93											
Average	70.20	0.52	8.65	7.99	0.35	0.11	0.47	6.03	4.39	0.04	1.24
2 s.d.	3.50	0.24	3.42	0.92	0.12	0.18	0.49	1.14	0.30	0.08	0.67

Errors are 2 s.d. calculated using replicate analyses of MPIDING StHs6/80 glass. A full grain-specific glass data set is presented in Supplementary Information 1.

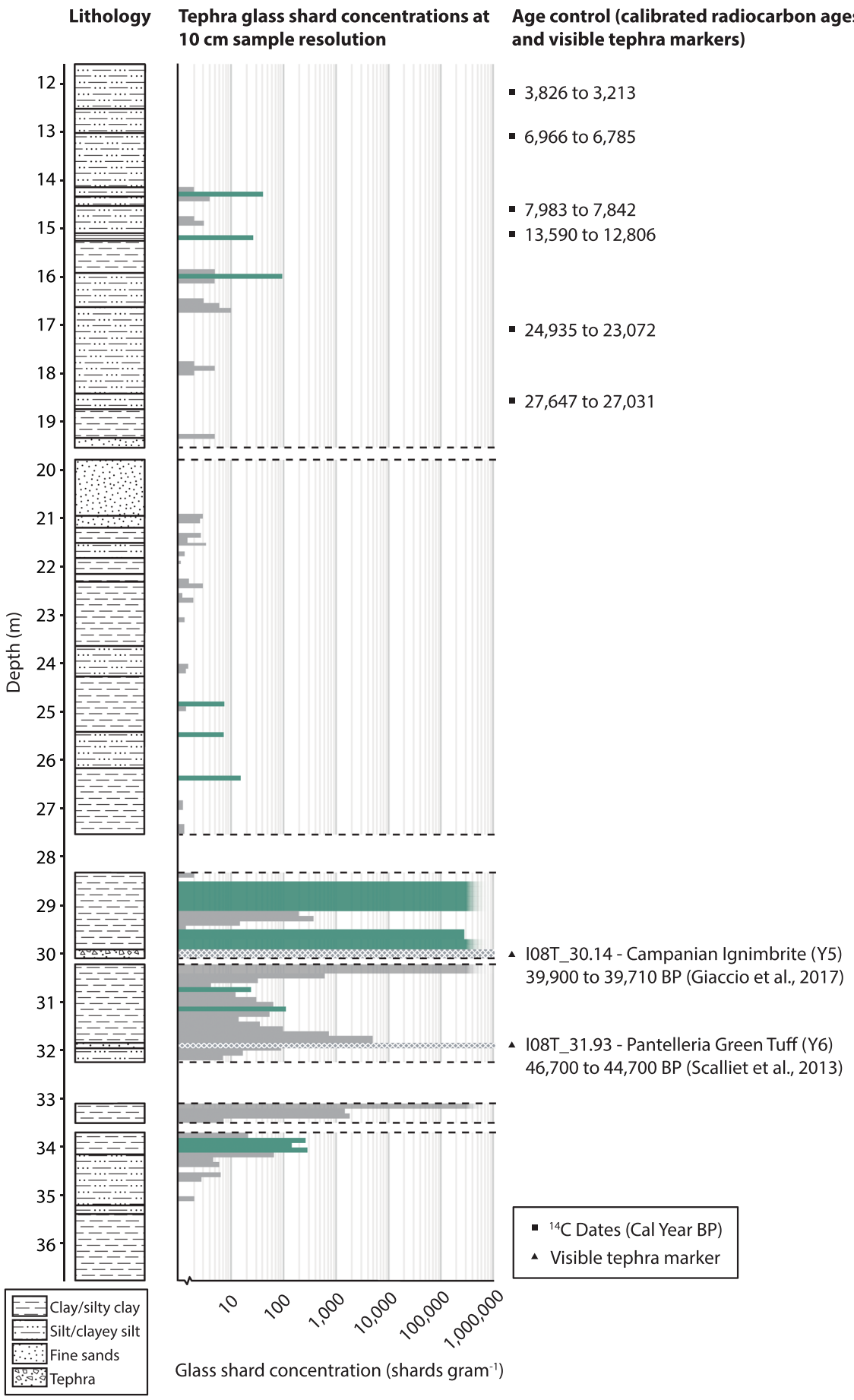

Figure 2. Results of low resolution (10 cm) rangefinder investigations of the I-08 core shown alongside ^{14}C dates from Jones *et al.* (2013), recalibrated using the IntCal20 calibration curve (Reimer, 2020). Green bars represent horizons selected for high resolution analysis. Note glass shard concentrations are displayed on a logarithmic axis. [Color figure can be viewed at wileyonlinelibrary.com]

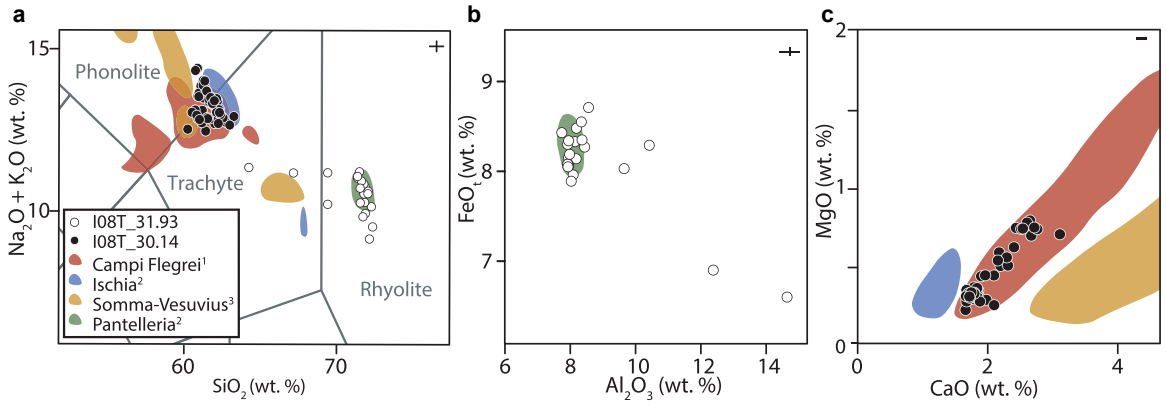

Figure 3. Major element geochemistry of tephra glass shards from visible tephra layers I08T_31.93 and I08T_30.14 compared to summary compositional envelopes from Italian volcanic centres that erupted trachytes, phonolites, and rhyolites during the last glacial cycle, including (a) total alkali vs. silica plot (Le Bas *et al.*, 1986) and major element biplots (b, c). Geochemical fields are based on proximal data from (1) Tomlinson *et al.* (2012), (2) Tomlinson *et al.* (2015) and (3) Tomlinson *et al.* (2015), for distal comparisons see Figs. S1 and S3. Errors are 2 s.d. calculated using replicate analyses of MPIDING StHs6/80 glass. [Color figure can be viewed at wileyonlinelibrary.com]

correlated to the eruption found thousands of kilometres from source (Pyle *et al.*, 2006).

On the basis of the correlation of I08T_30.14 to the CI (Y-5) tephra isochron (Table S7), the widely used $^{40}Ar/^{39}Ar$ and ^{14}C age of the CI 39.85 ± 0.14 ka BP (Giaccio *et al.*, 2017) is imported at the upper bound of the Campanian Ignimbrite visible tephra deposit, at 30.04 m depth in the I-08 core chronology (Fig. 2).

Cryptotephra

Rangefinder (10 cm contiguous sampling) investigations revealed 11 intervals of increased volcanic glass concentration which warranted further 1 cm resolution study (Fig. 2). Sections of the core were selected for high resolution study by identifying significant increases in the tephra glass shard concentration profile.

The depths selected for high resolution study in the I-08 core were:

- 34.11 to 33.81 m — Section 4.2.1
- 31.21 to 31.11 m; 30.71 to 30.81 m — Section 4.2.2
- 29.88 to 29.40 m; 29.00 to 28.51 m — Section 4.2.3
- 16.10 to 16.00 m; 15.30 to 15.20 m; 14.40 to 14.30 m — Section 4.2.4

Three further small peaks at ca. 26.3, 25.5 and 24.9m depth were also studied at 1 cm resolution, however, the results of these investigations are not included here as the shape of a shard concentration profiles and inconsistent morphologies of glass shards within these sections suggest post-depositional reworking rather than primary airfall of tephra. Due to a gap in the core between 32 and 33 m, associated with core extraction, the increase in glass shard concentration at ca. 33.1 m was not interrogated.

Pre-Pantelleria Green Tuff (>30.93 m depth; > ca. 46 ka BP)

Tephra glass shards were found in all but seven of the 1 cm samples studied between 34.11 and 33.81 m depth, albeit at low concentrations (<1, 50<1500 shards g^{-1}). Throughout this interval, glass shards were generally light olive in colour and of varying relief, with both fluted and cuspate forms. Shards were generally small, <40 µm on the longest axis, however, at 34.03 m depth larger shards (ca. 80–100 µm) accounted for ca. 5% of the total shards counted. In the sample at 33.85 m depth, a few shards containing microcrysts were identified. The highest concentration of tephra glass shards in this section of the core, with ca. 1600 shards g^{-1}, was found at 33.97 m depth.

Considering the distribution, appearance and size of the glass shards in each sample, five peaks in cryptotephra concentration were targeted for geochemical analysis (Fig. 4a) at 34.07, 34.03, 33.99, 33.97 and 33.85 m depth. WDS-EPMA analysis of shards in this section of core was challenging due to their small size, however, at least one analysis was possible for shards in three of samples, hereon I08T_34.02, I08T_33.97, and I08T_33.85.

I08T_34.02, I08T_33.97, and I08T_33.85 all have a tephra glass shard concentration ca. 200 shards g^{-1}. Glass shards in all three layers are geochemically similar (Fig. 4a), with a rhyolitic (SiO_2 > 70%) composition (Fig. 4b). All three tephra layers are peralkaline rhyolites, characterised by low Al_2O_3 between 8 and 12 wt.%. The FeO values (FeO_t ca. 8 wt.%) rule out Pantellerites from known eruptions of Nemrut Volcano in Eastern Turkey (Peretyazhko *et al.*, 2015), and thus the layers are likely derived from last glacial volcanism of Pantelleria.

There are three known widespread Mediterranean tephra isochrons of Pantellerian origin (Table S7), the ca. 46ka BP Pantelleria Green Tuff (Y-6; Scaillet *et al.*, 2013), the ca. 77 ka BP P-10 (Paterne *et al.*, 1988) and the older, ca. 131 ka BP, P-11 tephra marker (Paterne *et al.*, 2008). The P-10 tephra marker identified by Paterne *et al.* (1988), subsequently identified in Lago Grande di Monticchio (TM-22; Wulf *et al.*, 2004), Adriatic Sea core PRAD 1-2 (PRAD-2375; Bourne *et al.*, 2015) and correlated to the ca. 85 ka BP Proximal Ignimbrite Z of Pantelleria (Rotolo *et al.*, 2013), is typically associated with a NNW dispersal axis. Correlation to the P-10 tephra marker can be ruled out as these deposits are, at all sites, associated with higher Al_2O_3 and lower FeO_t values (Fig. 4) than the Ioannina tephra layers. The P-11 tephra marker has been identified in Greece, at Theopetra Cave (Karkanas *et al.*, 2014) and, putatively, at Megali Limni (Lesvos; Margari *et al.*, 2007; Vogel *et al.*, 2010. Correlation of the ML-5 tephra layer at Megali Limni to the P-11 tephra marker is uncertain as, whilst geochemically similar, the age of the P-11 eruption is difficult to reconcile with its stratigraphic position within the Megali Limni pollen record. Both the P-11 and ML-5 tephra deposits can be ruled out as correlatives as the FeO_t concentrations found in I08T_34.02, I08T_33.97 and

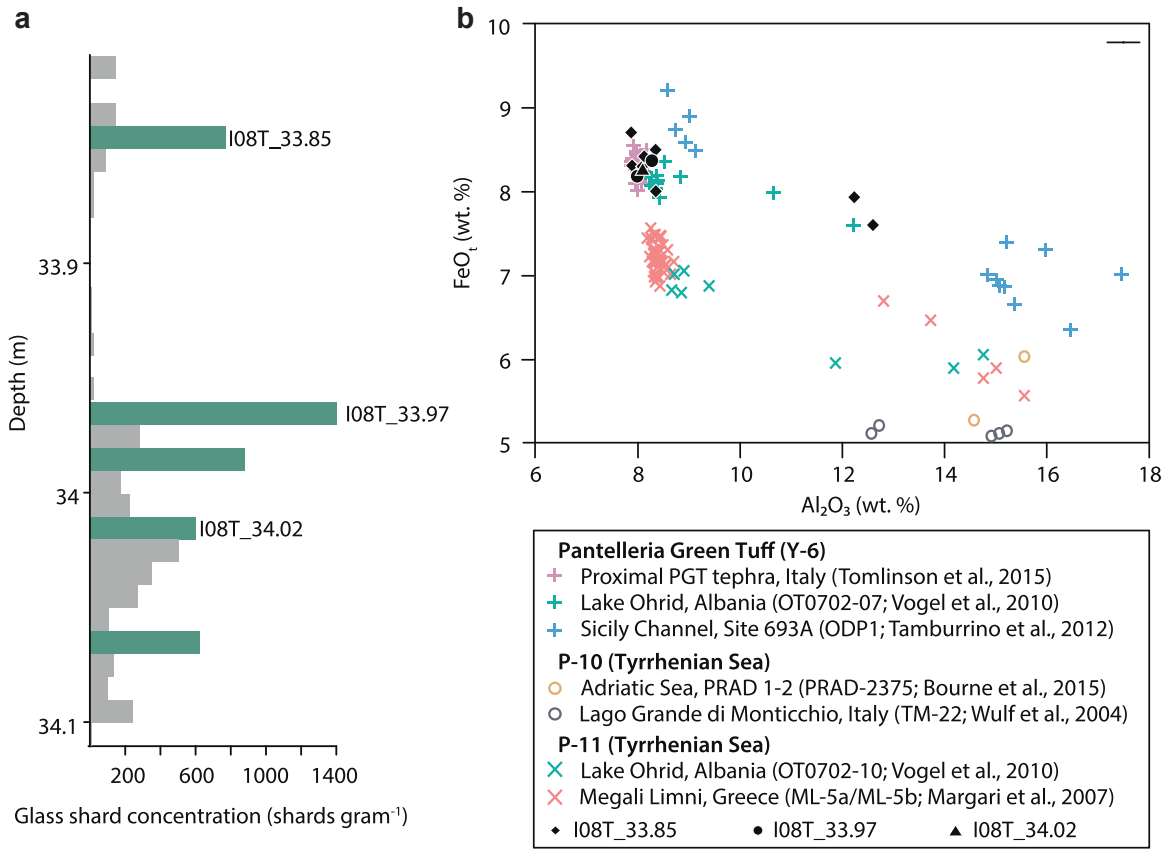

Figure 4. Tephra glass shard concentrations identified in sediments below the visible I08T_31.93 tephra marker (correlated to the Pantelleria Green Tuff). (a) Glass shard concentration against depth, horizons in green reflect depths prioritised for geochemical analysis and (b) Al_2O_3 vs. FeO_t biplot for the analysed Ioannina cryptotephra layers from this interval, alongside proximal and distal tephra layers associated with the Pantelleria Green Tuff eruption (+; pink)/Y-6 distal tephra (+; blue and green) and the P-11 distal tephra (x). Note: Margari *et al.* (2007) originally correlated ML-5 to the Y-6 eruption, however, here we utilise the revised correlation of Vogel *et al.* (2010); Hardiman (2012). Errors are 2 s.d. calculated using replicate analyses of MPIDING StHs6/80 glass. [Color figure can be viewed at wileyonlinelibrary.com]

I08T_33.85 fall considerably above the range of FeO_t in glass shards from the P-11 and ML-5 deposits (Fig. 4).

The geochemical affinity of glass shards in layers I08T_34.02, I08T_33.97, and I08T_33.85 leaves open the possibility that these layers are stratigraphically displaced contamination from the visible I08T_31.93 tephra layer either through post-depositional reworking, or coring-related displacement. The absence of tephra glass shards from a number of samples, for example, between 33.96 and 33.86 m depth, as well as the absence of tephra from the blank samples run during the extraction process rules out laboratory contamination during cryptotephra extraction and analysis.

Alternatively, tephra layers I08T_34.02, I08T_33.97, and I08T_33.85 may be coring artefacts, given that the borehole from which cores were retrieved would still have contained tephra from the I08T_31.93 visible deposit which may have been retrieved in subsequent core drives. Similar stratigraphic displacement of tephra glass shards has been identified in the TP-2005 core from Tenaghi Philippon, with glass shards associated with the Campanian Ignimbrite identified 22.78 m below the visible CI deposit, attributed by Wulf *et al.* (2018) to coring-related contamination. Particularly, following retrieval of a core drive the load of the water column in the borehole is suggested to have forced glass shards to depths of 20 cm or more into the upper part of the subsequent drive (Wulf *et al.*, 2018). In contrast to the peat-dominated Tenaghi Philippon sequence, the sediment matrix of the Ioannina I-08 core primarily consists of silts and clays, and thus the denser, more cohesive Ioannina cores should have reduced porewater, making the sediments less susceptible to such displacement. Furthermore, the glass shard distribution profiles (Fig. 4) do not support the coring-associated displacement hypothesis. If tephra glass shards were coring artefacts, it would be expected that from the top of the 70 cm core segment at 33.81 m depth water load should disperse shards throughout the stratigraphy. Instead, distinct peaks in glass shard concentration are observed at 21, 16 and 4 cm below the top of the core drive (I08T_34.02, I08T_33.97 and I08T_33.85 respectively).

The I08T_34.02, I08T_33.97 and I08T_33.85 cryptotephra peaks may represent smaller, previously unknown eruptions of Pantelleria. Much of our understanding of Pantellerian volcanism is based on the proximal stratigraphy and smaller eruptions from Pantelleria predating the large P-11 and Green Tuff (Y-6) deposits may not have been observed due to subsequent burial by more voluminous deposits. Whilst distal tephra study has been undertaken on visible units identified in marine sequences from the nearby Sicily Channel, very few detailed cryptotephra studies have been undertaken in the southern Mediterranean. Correlation of these tephra deposits to known volcanic events or tephra isochrons identified in other sequences is not possible at present.

Therefore, we suggest that tephra layers between 34.11 and 33.81 m depth in the I-08 core to genuine but previously unrecognised eruptions of Pantelleria, however, confirmation is needed by replication at another site.

Post-Pantelleria Green Tuff and Pre-Campanian Ignimbrite (31.93–30.14 m depth; ca. 46–40 ka BP)

Two intervals of increased glass shard concentration were identified for further study in the section of core bracketed by the visible I-08 tephra layers, I08T_31.93 and I08T_30.14,

which are correlated to the ca. 46 ka Pantelleria Green Tuff and 40 ka BP Campanian Ignimbrite respectively. Three depths within which glass shard concentrations peaked well above background, were identified and selected for geochemical analysis: I08T_31.19, I08T_31.17 and I08T_30.74 (Fig. 5a).

I08T_31.19 primarily of low relief, olive-coloured shards, with a concentration ca. 200 shards g^{-1}. Glass shards in I08T_31.19 are rhyolitic (SiO_2 from 72.3 to 74.1 wt.%) in composition, and demonstrate the diagnostic low Al_2O_3 associated with distal deposits from Pantelleria (Fig. 5b). Within this grouping there is some variation in Na_2O with values between 3.2 and 6.8 wt.%, however, values for FeO_t and K_2O are well clustered (Fig. 5c–e).

Whilst evidence exists for post-PGT eruptive activity at Pantelleria, a period of quiescence has been suggested following the PGT, ending at 35 ka BP with the eruption of the Serra di Ghirlanda tephra (Civetta *et al.*, 1984). In contrast, Mahood and Hildreth (1986) suggest that volcanism at Pantelleria resumes rapidly after the PGT eruption, identifying trachyte lavas from a vent at Monte Gibele which they date using K/Ar to ca. 41–27 ka BP, which would indicate that some eruptive activity occurred between the PGT and CI eruptions. However, no distal studies have yet identified tephra deposits associated with post-PGT Pantellerian volcanism that could provide a correlative for I08T_31.19.

Alternatively, I08T_31.19 may be the result of remobilisation of tephra glass shards associated with the I08T_31.93 tephra marker some 70 cm deeper in the core. Mechanisms that may have caused post-depositional reworking in the Ioannina cores will be discussed in greater detail in 'Discussion' section.

I08T_31.17 (just 2 cm above I08T_31.19) and I08T_30.74 contain low relief, colourless shards in concentrations ca. 275 and 180 shards g^{-1}, respectively. Tephra glass shards from both layers are phono-trachytic (SiO_2 ca. 62 wt.%) and have a geochemical signature that matches eruptions of the Campanian Volcanic Field (Fig. 5). The I08T_31.17 and I08T_30.74 compositions are indistinguishable from that of the Campanian Ignimbrite tephra layer (I08T_30.14), which occurs 60 cm above I08T_30.74 and ca. 1 m above I08T_31.17 in the Ioannina core (Fig. S4).

Multiple pre-CI eruptions have been recorded in both proximal and distal archives, including marine cores from the Adriatic (S7; Tomlinson *et al.*, 2012; Bourne *et al.*, 2010; Matthews *et al.*, 2015). Most notably, the tephra record from Lago Grande di Monticchio identifies at least four smaller-scale tephra markers associated with pre-CI volcanism from Campi Flegrei which occur ca. 600 varve years prior to the CI (Wulf *et al.*, 2004, 2008; Wutke *et al.*, 2015). The pre-CI LGdM tephra markers, termed the TM-18 tephras, are geochemically difficult to distinguish from the CI without high-precision trace element glass data (Wutke *et al.*, 2015). Of these markers Wulf *et al.* (2018) identify medial distal tephras TM-18-1d, TM-18-4, TM-18-9e as the most likely correlatives for pre-CI Campi Flegrei tephra horizons identified in distal settings. Tephra deposits associated with the TM-18 pre-CI sequence have been identified in a limited number of distal archives. TM-18-1d, for example, has been identified in the Tenaghi Philippon sequence (Wulf *et al.*, 2018). The geochemical fingerprint of the Ioannina tephra deposits can, however, be separated from many of these pre-CI deposits on the basis of K_2O/Na_2O (Fig. S4).

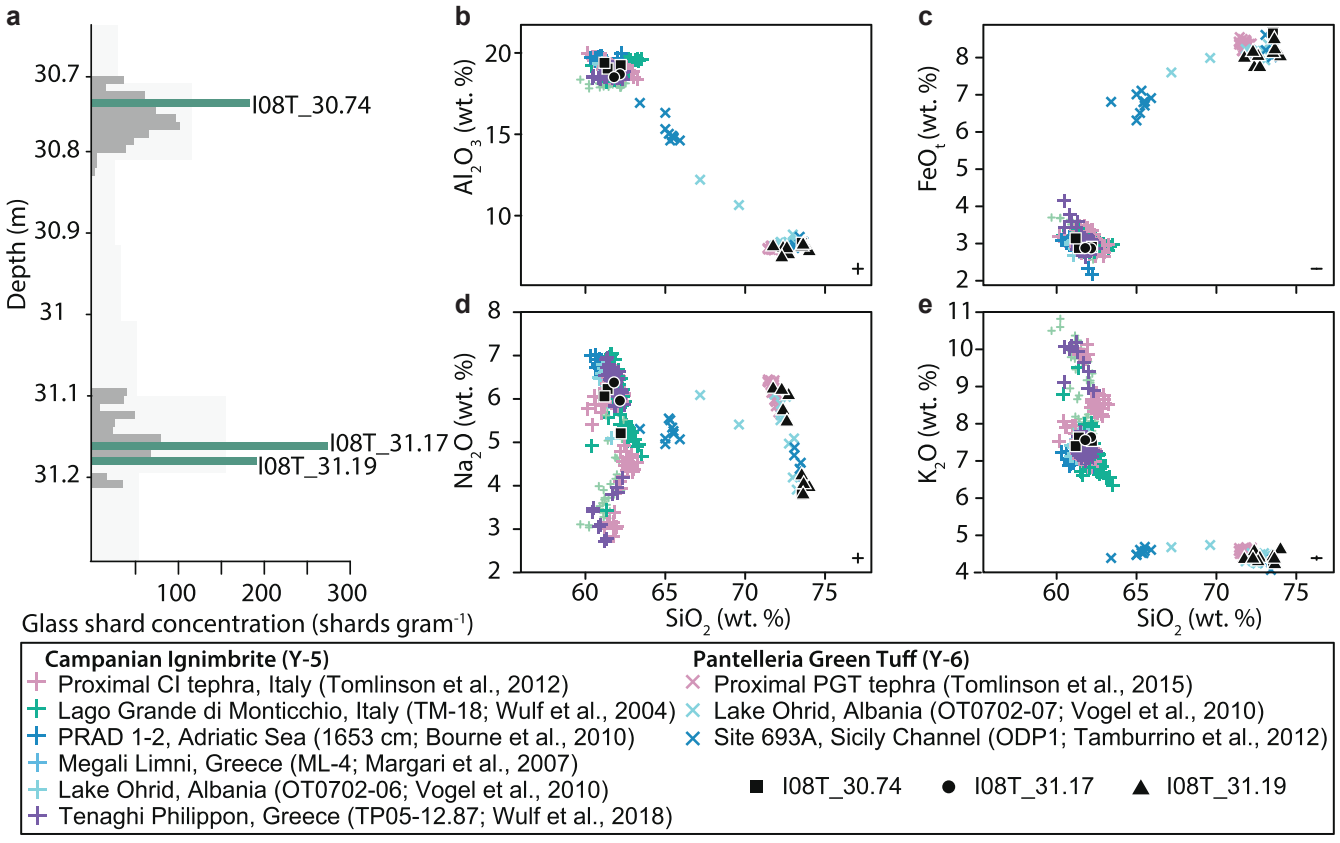

Figure 5. Cryptotephra peaks identified in sediments bracketed by the I08T_31.93 and I08T_30.14 tephra deposits (correlated to the Pantelleria Green Tuff and Campanian Ignimbrite respectively). (a) Glass shard concentration against depth and (b–e) major element biplots for Ioannina cryptotephra layers, alongside proximal and distal tephra layers associated with the Pantelleria Green Tuff and Campanian Ignimbrite eruptions. Errors are 2 s.d. calculated using replicate analyses of MPIDING StHs6/80 glass. [Color figure can be viewed at wileyonlinelibrary.com]

As with the ca. 33 m depth tephra markers, it is also possible that I08T_31.17 and I08T_30.74 are related to downcore displacement of tephra shards associated with the coring process. All the tephra deposits identified fall within the major element composition of the I08T_30.14 tephra deposit (Fig. S4), this explanation cannot be ruled out at present.

I08T_31.19, I08T_31.17 and I08T_30.74 are, at present, uncorrelated, however, they may represent distal deposits of 41–20 ka BP activity at Pantelleria (I08T_31.19) and Campi Flegrei (I08T_31.17 and I08T_30.74). Given their close geochemical match with the visible I08T_31.93 and I08T_30.14 tephra markers, however, it seems most likely that these layers represent post-depositional reworking of tephra glass shards (I08T_31.19).

Post-Campanian Ignimbrite (29.88–28.51 m depth; ca. 40–30 ka BP)

High resolution (1 cm) cryptotephra investigations were undertaken between 29.88 and 29.51 m depth and 29.01–28.51 m depth. The section of core between 29.51 and 29.01 m depth, where glass shard concentrations fell below 100 shards g^{-1} in rangefinder investigations, was not studied further (Fig. 2). The hiatus in tephra deposition between 29.51 and 29.01 m, observed via cryptotephra analyses, is verified by the XRF scanning data. XRF-derived elemental ratios for bulk sediment, most notably the K/Ti ratio, closely tracks tephra glass shard concentration throughout this section of the core (Fig. 6b).

Three abrupt increases in glass shard concentration relative to the underlying sample were observed at 29.72, 29.65 and 29.62 m depth, which is above the I08T_30.14 CI tephra marker but below the hiatus in shard deposition at 29.51 m depth (Fig. 6a). Whilst peaks in glass shard concentration at 29.65 and 29.62 m depth are lower than peaks at 29.83 and 29.72 m depth, tephra glass shard concentrations at 29.65 and 29.62 m depth (ca. 5×10^5 and 11×10^5 shards g^{-1} respectively) represent large increases relative to the underlying samples (Fig. 6a). Glass shards at all depths generally measured between 60 and 100 µm on the longest axis. At 29.72 m depth, however, shards were much larger, typically ca. 100 µm on the longest axis (Fig. 6c).

A fourth sample at 29.83 m depth, was investigated as a potential primary ash-fall horizon on the basis of shard morphology as, similarly to the sample from 29.72 m depth, shards in this sample were far larger than in surrounding tephra samples, typically >100 µm on the longest axis (Fig. 6c). Glass shards throughout this section of core were generally colourless, of low relief, and largely consisted of platy forms, however, shards with a range of other morphologies, including fluted and cuspate shards, were also present.

A distinct increase in tephra glass shard concentration is observed at 28.98 m depth and is also identifiable through a peak in the K/Ti XRF ratio as well as a coarsening in the particle size data. Above 28.98 m there is a return to glass shard concentrations ca. 1×10^5 shards g^{-1} until 28.83 m depth, at which point concentrations begin to increase, albeit with a number of sharp jumps and oscillations in glass shard concentration. The increase in tephra glass shard concentration throughout this section of the core correlates with an increase in K/Ti ratio (Fig. 6b), reflected in the particle size data as an increase in the frequency of particles in the 100–200 µm fraction (Fig. 6c).

Above the peak at 28.98 m depth, a further six samples were investigated since they show a large increase in glass shard concentration relative to their underlying sample (Fig. 6a). Observed glass shard morphologies are broadly consistent in samples between 29.01 and 28.51 m depth, with shards largely low relief, colourless, and dominated by platy, curvilinear, and cuspate forms. A change in glass shard morphology is observed in at 28.66 m depth, where shards display an increase in ventricular features, microcryst inclusions with a limited number of shards ($n = 2$) with pumicious forms. Due to a return to platy, low relief shards in samples above 28.66 m

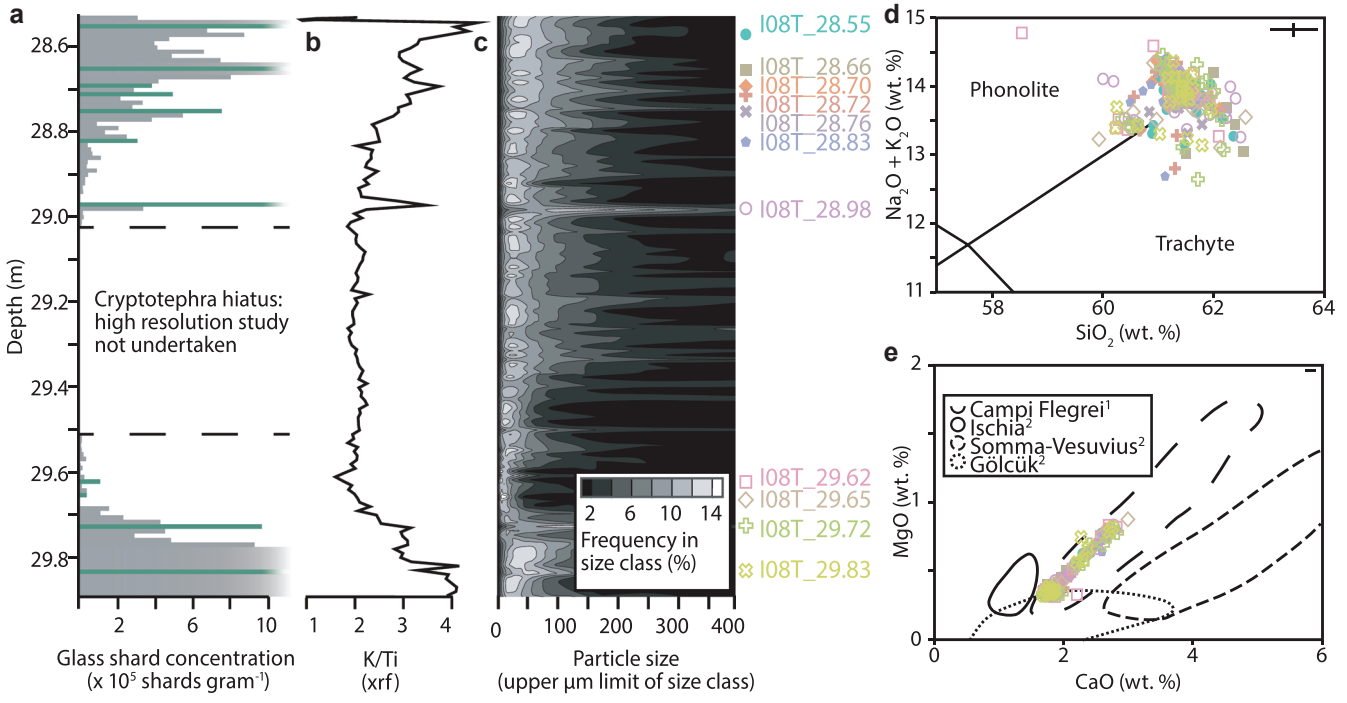

Figure 6. Results of high-resolution (1 cm) cryptotephra analysis between 29.88 and 28.51 m depth, showing: stratigraphic plot of (a) glass shard concentrations, (b) XRF-derived K/Ti ratio, and (c) bulk particle size distribution of the I-08 core. Also shown are major and minor element geochemistries of tephra glass shards from cryptotephra peaks, including (d) total alkali vs. silica plot (Le Bas *et al.*, 1986) and (e) CaO vs. MgO showing geochemical fields based on data from (1) Tomlinson *et al.* (2012) and (2) Tomlinson *et al.* (2015). Errors are 2 s.d. calculated using replicate analyses of MPIDING StHs6/80 glass. [Color figure can be viewed at wileyonlinelibrary.com]

depth, this influx of new morphologies may reflect primary airfall, henceforth the I08T_28.66 tephra deposit. Most shards observed in the 29.88–28.51 m interval were between 30 and 50 µm on their longest axis, however, occasional larger shards (up to 200 µm on the longest axis) were noted throughout the section.

Geochemical analysis of the 11 potential primary airfall tephra layers between 29.99 and 28.51 m depth characterises glass shards as phono-trachytic, with limited variability in SiO_2 (between 60 and 63 wt. %). CaO (1.1–2.8 wt. %) and MgO (0.2– 0.9 wt.%) values are consistent (Fig. 6b) Glass shards from all 11 depths are phono-trachytic (Fig. 6a). Post-CI (<40 ka BP) Mediterranean tephra deposits with phono-trachytic glass compositions may correlate to eruptions from the Campanian Volcanic Zone (trachytic and phonolitic; Tomlinson *et al.*, 2015), Gölcük (trachytic and phonolitic; Tomlinson *et al.*, 2015) and Mt. Etna (trachytic; Albert *et al.*, 2013). The MgO and CaO concentrations of all 11 Ioannina tephra deposits between 29.99 and 28.51 m depth indicate that they are all associated with eruptive activity from Campi Flegrei (Fig. 6e).

Two possible explanations for the unusual stratigraphic distribution of tephra glass shards through this section of the core are suggested. The first is that the peaks, which are often characterised by abrupt increases in glass shard concentration relative to the underlying deposits, are primary air-fall deposits associated with post-CI eruptions in the Mediterranean. The second is that these peaks represent a complex process of post-depositional reworking of the Campanian Ignimbrite tephra deposit in the Ioannina basin. It should be noted that the two explanations presented here are not mutually exclusive and it is possible that both reworking and the complex eruptive history of Campi Flegrei act in concert to produce the complex tephra record in this section of the I-08 core. Both possible interpretations of the I-08 tephra record are further discussed in 'Discussion' section.

Last Glacial to Interglacial Transition (16.20–14.20 m depth; ca. 25–7 ka BP)

Three discrete peaks in cryptotephra glass shard concentration (I08T_16.07, I08T_15.23 and I08T_14.39) are located between 16.20 and 14.20 m depth in the I-08 core. This section overlies the coarse sand deposits associated with low lake levels during the last full glacial (MIS2, ca. 22 ka BP) and shown by Jones *et al.* (2013) to cover the Last Glacial-Interglacial Transition (LGIT). In contrast to tephra peaks between 29.88 and 28.51 m depth peaks I08T_16.07, I08T_15.23 and I08T_14.39 are isolated, with no tephra glass shards found in the overlying and underlying sediments. We can rule out coring-related displacement for I08T_16.07 and I08T_14.39 as these isochrons are 17 and 59 cm from the top of their core sections respectively. We are also confident that the isolated peak at I08T_15.23 does not represent coring-related stratigraphic displacement as, whilst glass shards are identified in the 1 cm samples above and below the core, no shards are present in the samples which bound these, suggesting cryptotephra glass shards form a distinct layer within the stratigraphy. Therefore, we are confident that these are independent isochrons.

Shards from I08T_16.07, I08T_15.23 and I08T_14.39 are highly evolved rhyolites (Fig. 7b) characterised by high SiO_2 values from 75.1 to 75.7 wt.% and total alkalis from 8.3 to 9.3 wt.%. Mediterranean volcanic centres which produce highly evolved rhyolites include the Aeolian Islands (notably Lipari and Salina; Albert *et al.*, 2017), Santorini (Tomlinson

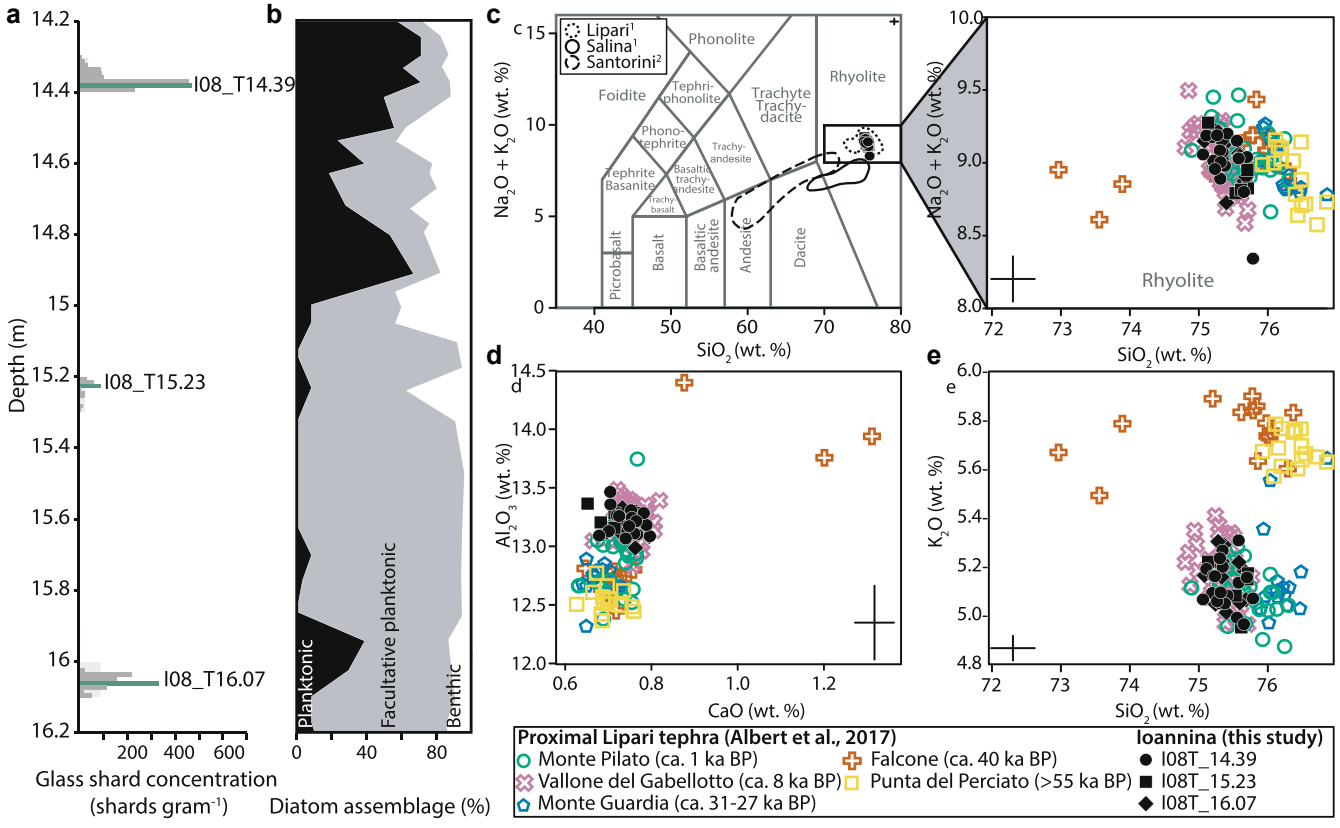

Figure 7. Identified cryptotephra peaks between 16.20 and 14.20 m depth in the I-08 core, showing (a) glass shard concentration against depth, (b) diatom assemblages from Jones *et al.* (2013) showing the Late Glacial to Early Holocene transition in the I-08 core, (c) total alkali vs. silica plot (Le Bas *et al.*, 1986), geochemical fields are based on data from (1) Albert *et al.* (2017) and (2) Satow *et al.* (2015) (d, e) major element biplots for Ioannina Late Glacial cryptotephra layers alongside the major element compositions of proximal deposits associated with Lipari volcanism (Albert *et al.*, 2017). [Color figure can be viewed at wileyonlinelibrary.com]

et al., 2015) and Acigöl (Tryon *et al.*, 2009). Reference compositional data from these volcanic centres are compared to the Ioannina LGIT tephra compositions in Fig. 7. The Ioannina LGIT tephra correlate well to high-K calc-alkaline activity at Aeolian Island volcano Lipari. Multiple eruption phases have been identified in the proximal Lipari record duing the last glacial cycle, some of which are indistinguishable based on their major element geochemistry (Albert *et al.*, 2017). However, the Vallone del Gabellotto eruptive cycle (*sensu.* Albert *et al.*, 2017), which is dated to ca. 8 ka BP (Caron *et al.*, 2012; Siani *et al.*, 2004), provides the only likely LGIT correlative for the Ioannina tephra markers (Fig. 7).

Of particular note is the widespread Vallone del Gabellotto (VG/E-1) tephra dated to 8630–8430 cal years BP using the IntCal20 calibration curve (Fig. S7). The VG/E-1 tephra has been correlated to horizons present in Tyrrhenian, Ionian, and Adriatic marine cores (Albert *et al.*, 2017) as well as Tenaghi Philippon in NE Greece (Wulf *et al.*, 2018). Of the three Ioannina LGIT tephra deposits the most likely correlative for this widespread Holocene tephra marker is the uppermost I-08 tephra layer, I08T_14.39, the only tephra deposit that sits within the Holocene section of the core (Fig. 7b). The correlation of I08T_14.39 with the Vallone del Gabellotto (E-1) isochron is further supported by new trace element analysis, Supplementary Information 1. Fig. 8 shows good correspondence between I08T_14.39, three proximal deposits of the Vallone del Gabellotto, and its distal correlative M25/4-12-28cm tephra from the Ionian Sea (Albert *et al.*, 2017).

The proximal Lipari record does contain eruptive deposits of LGIT age, however, these are 'localised' and not traced widely across the island (Albert *et al.*, 2017). In the distal realm an older layer with a Gabellotto-like Lipari composition has been recorded at 44 cm depth in the Ionian Sea core M25/4-12 (Albert *et al.*, 2013). The lowermost Ioannina LGIT tephra layer, I08T_16.07, has a trace element geochemistry that corresponds well to the distal Ionian Sea tephra marker M25/4-12-44 cm, which has yet to be linked to a proximal deposit. Therefore, we propose a tentative correlation of I08T_16.07 to Ionian Sea tephra marker M25/4-12-44 cm, which does not yet have a correlative in the proximal tephrostratigraphy. The identification of this tephra marker ca. 500 km from source is currently the most distal deposit and the first outside of Italy and the surrounding seas.

The intermediate Ioannina LGIT tephra, I08T_15.23, has yet to be correlated to a proximal or distal isochron, however, has distinctly lower Th, La, Eu and Ce concentrations (Fig. 8a) than the other tephra layers and is thus likely to be the product of a separate eruption. Therefore, I08T_15.23 has the potential to provide an additional stratigraphic marker in the future.

On the basis of the correlation of I08T_14.39 to the E-1 tephra isochron, the uncalibrated ^{14}C age of this marker, 7.77 ± 0.04ka BP (Caron *et al.*, 2012; Albert *et al.*, 2017), is imported to this depth in the I-08 core chronology and recalibrated as part of the OxCal P_Sequence.

Discussion

The Campanian Ignimbrite tephra marker

The I08T_30.14 tephra deposit, which we correlate to the 39.85 ka BP campanian Ignimbrite eruption of Campi Flegrei

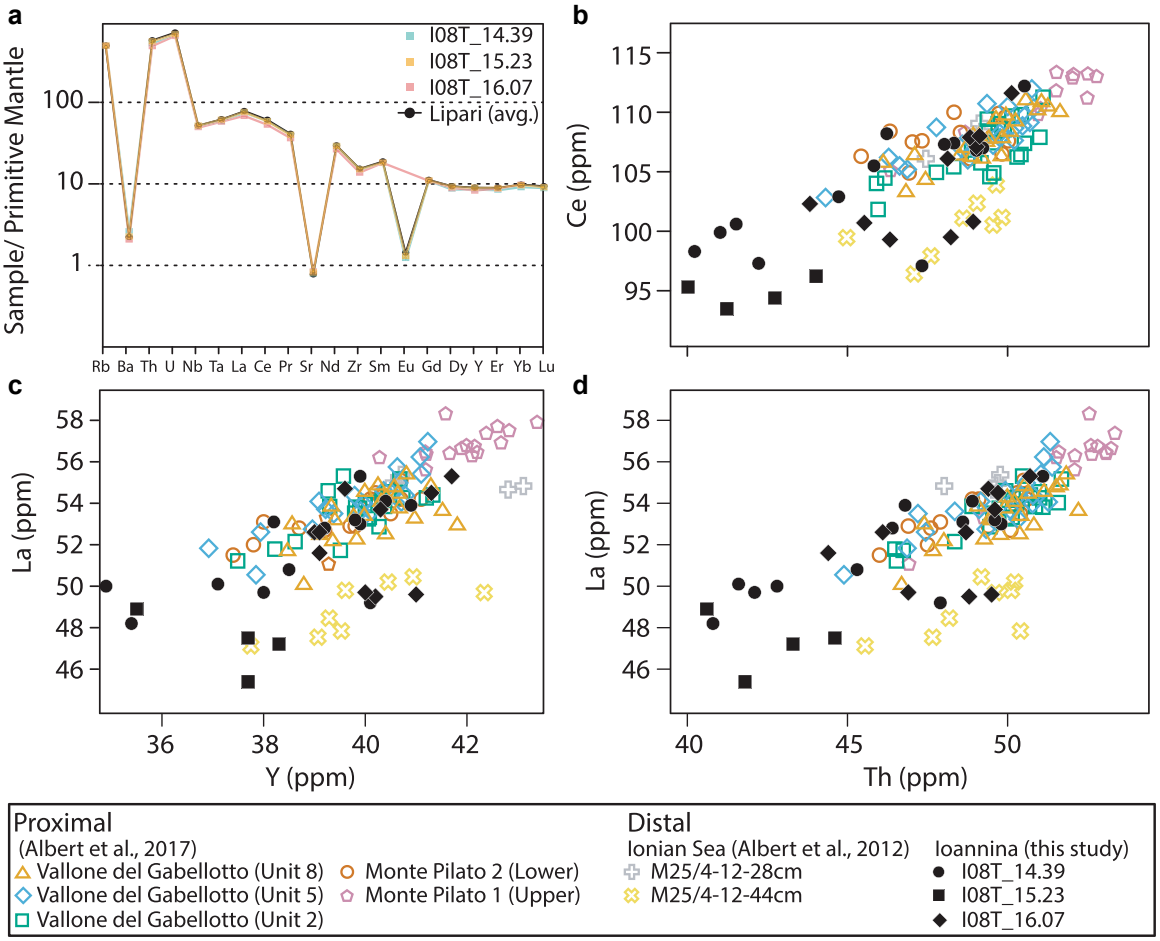

Figure 8. Trace element analysis of I-08 tephra layers I08T_16.07, I08T_15.23 and I08T_14.39 plotted against Lipari proximal and Ionian Sea distal tephra deposits from (Albert *et al.*, 2017), including: (a) average mantle normalised (Sun & McDonough, 1989) trace element profiles and (b–d) trace element biplots. [Color figure can be viewed at wileyonlinelibrary.com]

caldera, Italy, is interesting as it contains the full major and minor element variation observed in the CI proximal deposit (Fig. S3; Table S7). Two closely-related compositional groups can be recognised within the I08T_30.14 tephra deposit, illustrated by differences in CaO, MgO and K_2O at overlapping SiO_2 concentrations (Fig. S3). The two composition groups in I08T_30.14 closely correspond to the end member associated with the lower and intermediate fall deposits of the CI eruption in the proximal deposits (CaO <2; K_2O < 8; Na_2O > 5), as well as as the higher CaO and K_2O and lower Na_2O end member associated with the upper flow (Tomlinson *et al.*, 2012). Of the distal occurrences of the CI/Y-5 tephra this upper flow end member is only identified in Megali Limni, Tenaghi Philippon, and Kalodiki (Greece; Pyle *et al.*, 2006; Margari *et al.*, 2007; Wulf *et al.*, 2018) and the archaeological site of Crvena Stijena (Montenegro; Morley & Woodward, 2011). Elsewhere tephra deposits associated with the CI eruption, for example, in PRAD 1-2 (Adriatic Sea; Bourne *et al.*, 2010) and Lake Ohrid (Albania/Montenegro; Vogel *et al.*, 2010), have chemical compositions which more closely match the lower and intermediate fall deposits. The offset in glass geochemical composition of the CI/Y-5 tephra layer between these different sites may arise from a variety of factors, including the height of the volcanic plume at different stages of the eruption, the prevailing wind direction, and the varying atmospheric transport and deposition of tephra glass shards due to differences in the eruption dynamics (e.g. injection height, wind speed, volume) and physical properties between glass shards generated in different phases of the eruption.

With regards to the thickness of the Ioannina I08T_30.14 (CI/Y-5) deposit, estimates from the Costa *et al.* (2012) ash fall out model for the Campanian Ignimbrite suggest that a ca. 10 cm deposit is expected at the site. That the deposit in the I-08 sequence, at even the lowest estimate for layer thickness, exceeds the model estimate is likely related to site-specific factors. The increased thickness of the I-08_30.14 layer is not without precedent. In their work mapping the thickness of the CI/Y-5 tephra marker Engwell *et al.* (2014) argue that in distal subaerial environments deposits are typically thicker than for equivalent deep sea deposits. Primarily, the large scale of the Ioannina catchment means large volumes of tephra would have been deposited into the lake environment through subsequent in-wash processes. Post-depositional reworking of unconsolidated tephra deposits from the surrounding landscape, facilitated by the steep topography, seems likely in the Ioannina basin and may have led to the redeposition of sediments in the lake.

Interpreting the post-CI tephra record

Here we consider two interpretations of the tephra distributions outlined in 'Post-Campanian Ignimbrite (29.88–28.51 m depth; ca. 40–30 ka BP)' section, in sediments from 29.88 to 28.51 m depth which postdate the 39.85 ka Campanian Ignimbrite eruption. First we consider the evidence that peaks in tephra glass shards represent primary air-fall of post-CI eruptive activity at Campi Flegrei. Second, we argue that they may represent reworking of tephra within the Ioannina catchment as well as within the lake basin itself.

Primary air-fall

Multiple post-CI last glacial tephra layers have been identified in the proximal Campi Flegrei stratigraphy, often termed the 'Tufi Biancastri' sequence (Table S7). Discriminating these eruptions in distal archives is challenging, however, given their close, often overlapping, glass shard geochemical compositions (e.g. Paterne *et al.*, 1988). Within the caldera, Tufi Biancastri tephra deposits have been identified at Verdolino (the ca. 28 ka BP VRb and ca. 30 ka BP VRa; Pappalardo *et al.*, 1999), and Trefola (the <38 ka BP TLo; Tomlinson *et al.*, 2012). At Ponti Rossi, to the northeast of the caldera, the Masseria del Monte Tuff (MdM), associated with a large VEI 6 eruption ca. 30 ka BP, has recently been correlated with the widespread Y-3 marine tephra (Albert *et al.*, 2019). The MdM/Y-3 tephra marker has been identified at a range of sites throughout the Mediterranean, including at Tenaghi Philippon (Wulf *et al.*, 2018), to the east of the Ioannina site. Additionally, a number of extra-caldera outcrops linked to post-CI activity at Campi Flegrei have also been identified; most notably the SMP1-e and CE-1 deposits (Sulpizio *et al.*, 2003; Albert *et al.*, 2015).

In the distal realm, a range of post-CI tephra markers associated with eruptions of Campi Flegrei have been described that have not been correlated to an eruption identified within the proximal stratigraphy (Table S7). At the nearby Lago Grande di Monticchio the TM-17-2 tephra, associated with post-CI volcanism at Campi Flegrei, is dated at 35530 ± 1780 varve years BP. Further afield, sediment cores from the Adriatic Sea Matthews *et al.* (2015) highlight a layer consisting of both trachytic and rhyolitic shards, termed SA03-11-T1535 (Table S7). The trachytic component of SA03-11-T1535 is chemically trachytic component is chemically identical to the Campanian Ignimbrite, but the stratigraphic position and association to the rhyolitic component of the marker lead (Matthews *et al.*, 2015) to argue a link to the CI eruption is implausible. The SA03-11-T1535 tephra marker correlates with a post-CI tephra marker reported in the Ionian Sea and the replication of the bimodal rhyolitic and trachytic chemical signature indicate it to be a distinctive layer from a single eruption event. The absence of any rhyolitic component in the post-CI cryptotephra peaks observed in the I-08 record mean that we can not identify a correlative with SA03-11-T1535.

The I08T_30.14 visible tephra marker has a broad geochemical composition, containing not only the low CaO, MgO and FeO_t and high Na_2O end members of the CI fall and the lower and intermediate flow units, but also the raised K_2O, lower Na_2O end member associated with the upper flow in the proximal stratigraphy (Table S7; Tomlinson *et al.*, 2012). All of the analysed tephra deposits which postdate the I08T_30.14 tephra marker have major and minor element geochemical compositions which fall within the envelope of the I08T_30.14 (Fig. S5) and, therefore, may represent reworked material from this deposit. Perhaps the most diagnostic component of the Campanian Ignimbrite tephra marker, which helps to discriminate it from other post-CI eruptions, is the upper flow end member (Tomlinson *et al.*, 2012). Thus, I-08 tephra layers which contain glass shards with upper flow-like compositions are likely to be reworked CI from the catchment (Fig. S5).

As a result of the broad geochemical composition of the I08T_30.14 tephra marker, identifying subsequent eruptions is challenging. For example, second to the CI, the most widespread last glacial tephra marker from Campi Flegrei is the ca. 30 ka BP Y-3 stratigraphic marker correlated by Albert *et al.* (2019) to the proximal Masseria del Monte Tuff. Across the full range of major and minor elements the geochemical fingerprint of the Y-3 tephra marker falls within the envelope of the I08T_30.14 (Fig. S6). It is possible to differentiate the markers, however, through FeO_t wt.% and the bimodal K_2O distribution associated with the MdM/Y-3 deposit (Fig. S6).

The geochemical composition of the I08T_28.98 tephra horizon does not match the MdM/Y-3 across the full major element geochemical assemblage of the Y-3 (Fig. S6) yet nor

does the I08T_28.98 perfectly match the geochemistry of I08T_30.14. Given the difference in composition between the I08T_28.98 cryptotephra layer and the I08T_30.14 (CI/Y-5) deposit, the I08T_28.98 is suggested to represent a post-CI primary air-fall deposit, although correlation is not possible at this stage. Future trace element analysis may provide a means of discriminating primary tephra inputs associated with post-CI volcanism from reworked material associated with the Campanian Ignimbrite and I08T_30.14 tephra markers.

Reworking

The presence of glass shards with geochemical compositions unique to the CI is the primary indicator that peaks in glass shard concentration overlying the I08T_30.14 (CI/Y-5) are most likely the products of the remobilisation of this tephra marker (Fig. S5). Specifically, glass shard compositions that match the products of the lower and intermediate flow (*sensu.* Tomlinson *et al.*, 2012), characterised by low CaO, MgO, and FeO_t and high Na_2O concentrations are unique identifiers of the reworked material.

The profile of glass shard concentrations against depth further suggests reworking, particularly in the upper layers (<28.8 m depth). In low energy lake sediment sequences primary air-fall tephra inputs are typically associated with a distinct peak followed by a decrease in the overlying sediments (Davies, 2015). The gradual increase in glass shard concentration between 28.97 and 28.66 m depth in the I-08 core does not suggest a primary input and could instead be interpreted as a gradual change in the sedimentary regime in the catchment.

A particular feature of this section of the core is the presence of shell layers absent from the underlying sediments. The presence of intervals within the Ioannina sediment sequence that contain molloscan faunal remains are argued to reflect lake-level variation (Frogley *et al.*, 2009). Molluscan shells are preserved in the sediment above ca. 29.9 m, suggesting that water levels were decreasing at the time of deposition. Tephra material at the lake margins would have been subaerially exposed following lake level lowering, then remobilised and deposited further into the lake basin, including to the I-08 core site. Such a process is consistent with the trend of gradual increase in tephra glass shard concentrations between 29.88 and 28.51 m depth (Fig. 9).

Alternatively, the recurrent nature of tephra remobilisation suggested by the stratigraphy of glass shard distributions (Fig. 6a), which shows pulses of increased glass shard concentration, may reflect surface run-off from a continuously eroding catchment. Lake Ioannina is primarily groundwater-fed and located in a basin largely bounded by steep slopes; thus it seems unlikely that processes of alluvial erosion and deposition are responsible for the recurrent inputs of reworked tephra.

A final mechanism which may explain the remobilisation of tephra deposits associated with the Campanian Ignimbrite eruption in the I-08 core may be that the redeposited tephra layers reflect a regional, extra-basin, erosional signal. Reworking of the Campanian Ignimbrite tephra layer has been identified in both the Tenaghi Phillipon (Wulf *et al.*, 2018) and Kopais (Hardiman, 2012) Greek cryptotephra records. Remobilisation of tephra deposits is becoming increasingly recognised as an important stage in the taphonomy of volcanic ash (Dominguez *et al.*, 2020; Buckland *et al.*, 2020) and the Campanian Ignimbrite deposit, widespread and deposited contemporaneously to the dry stadial conditions associated with Heinrich stadial 4, would likely have been frequently eroded and remobilised from the land surface. Indeed, tephra associated with the Campanian Ignimbrite eruption is found in aeolian sequences as far afield as Ukraine (Melekestsev *et al.*, 1984) and Romania where deposits of the tephra >1 m thick have been identified (Fitzsimmons *et al.*, 2013). It is therefore possible that aeolian remobilisation of tephra material may also be reflected in the Ioannina record, however, as noted, little evidence exists of geochemical alteration of tephra which would be expected if tephra has been remobilised from exposed environments.

To summarise, the consistent geochemical signal of glass shards deposited within the I-08 core between 29.88 and 28.51 m depth suggests erosion and redeposition of Campanian Ignimbrite tephra into the lake from the wider Ioannina catchment and the lake basin edges. Remobilisation appears to take place in two phases representing at least two separate processes. The shape of the shard concentration profile, which gradually decreases, suggests that immediately above the visible I08T_30.14 (CI) deposit, from 29.92 m through to 29.70 m depth tephra input is related to erosion of primary tephra fall from the Campanian Ignimbrite eruption within the Ioannina catchment. Subsequently, a hiatus in tephra deposition is interpreted as reflecting landscape stabilisation, with tephra deposits are no longer exposed to processes of surface run-off. The hiatus is clear in both the XRF data as well as the tephra glass shard concentration (Fig. 6a–c). We suggest the I08T_28.98 tephra marker, which is constrained to a 2 cm depth interval, is a primary air-fall deposit associated with Tufi Biancastri volcanism at Campi Flegrei caldera, however, we cannot yet correlate this tephra deposit to a specific eruption. From ca. 28 m depth upwards, there is a change in the sedimentary regime at the I-08 core site, which we interpret as a reduction in lake level resulting in the remobilisation of tephra material from the exposed lake margins. Extra-basin inputs from either aeolian remobilisation of exposed tephra surfaces or subsequent primary air-fall tephra inputs cannot be ruled out, however, given hiatuses in deposition of tephra glass shards, are unlikely to act as the dominant processes driving tephra deposition.

Age-depth model

The identification of the Pantelleria Green Tuff (Y-6) and Campanian Ignimbrite (Y-5) tephra markers within I-08

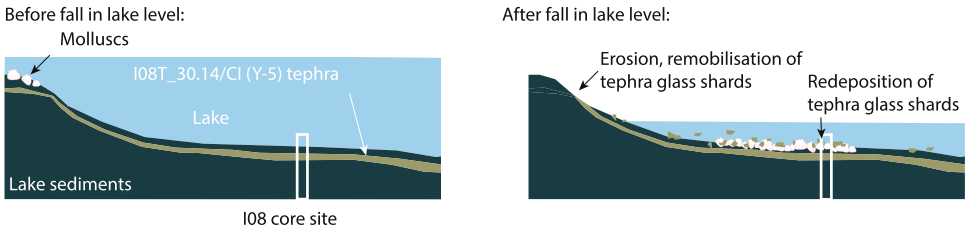

Figure 9. A schematic showing how a fall in lake level, also suggested by the presence of molluscan fauna within the I-08 core at the same depths, may have facilitated tephra reworking within the Ioannina catchment. [Color figure can be viewed at wileyonlinelibrary.com]

provides an opportunity to extend the chronology of Jones *et al.* (2013) back to ca. 45 ka BP. Furthermore, the identification of the Vallone del Gabellotto (E-1) provides an opportunity to refine the Holocene chronology of the I-08 core. Here we present a revised I-08 age-depth model which incorporates the three new tephra ages (Table 2; Fig. 10). The new full core-length age model incorporates earlier radiocarbon dates from macrocharcoal samples and compound-specific radiocarbon analysis (CSRA) for the upper section of the core (Jones *et al.*, 2013). The uncalibrated radiocarbon age estimate for the E-1 marker (Caron *et al.*, 2012) is recalibrated using IntCal20 as part of the OxCal model. Visible tephra deposits are most likely deposited over the course of days and weeks as opposed to years, therefore the 18 cm thick I08T_30.14 deposit is treated as an event horizon in the age model. The 39.85 ± 0.14ka age for the CI eruption is input at the lower (30.14 m) and upper (29.96 m) bounds of the I08T_30.14 tephra.

The new age model provides age estimates for the uncorrelated Aeolian Island tephra markers, I08T_16.07 and I08T_15.23, dated here to 12.46–10.21 ka BP and 10.65–8.52 ka BP, respectively, Fig. 10b,c. The ca. 11 ka BP age for I08T_16.07 further supports the proposed correlation of that layer to the Ionian Sea tephra marker M25/4-12-44cm Ionian Sea tephra marker, which occurs in sediments of Late Glacial age within the M25/4-12 core oxygen isotope stratigraphy (Negri *et al.*, 1999; Albert *et al.*, 2017).

Implications of the Ioannina tephra record

Regional tephra correlations

Three widespread tephra horizons have been identified in the Ioannina sequence: the Pantelleria Green Tuff (PGT/Y-6), the Campanian Ignimbrite (CI/Y-5), and the Vallone del Gabellotto (VG/E-1), facilitating direct correlation of the Ioannina I-08 sequence with regional palaeoecological and palaeoclimatic reconstructions from different environmental contexts (Fig. 11).

The ca. 40 ka BP CI/Y-5 tephra layer in the Ioannina record permits correlation to key southern European terrestrial palaeoenvironmental records, such as Lago Grande di Monticchio, Italy (Allen *et al.*, 1999; Wulf *et al.*, 2004), Lake Ohrid, Albania/Montenegro (Vogel *et al.*, 2010; Leicher *et al.*, 2016) and Tenaghi Philippon, Greece (Müller *et al.*, 2011; Wulf *et al.*, 2018), as well as central and eastern Mediterranean marine proxy records including cores from the Ionian (Keller *et al.*, 1978; Albert *et al.*, 2012), Tyrrhenian (Paterne *et al.*, 1988), Adriatic (Bourne *et al.*, 2010), Aegean (Keller *et al.*, 1978; Satow *et al.*, 2015) and Black Seas (Cullen *et al.*, 2014). The CI/Y-5 marker can be used

Table 2. Ioannina core I-08 tephra layers, and most widely used dates associated with their marine and distal correlatives.[1]

	Correlative				
Ioannina tephra	Proximal	Distal	Eruption age (ka)	Method	Reference
I08T_14.39	Vallone del Gabellotto	E-1	7.77 ± 0.04	^{14}C	Caron *et al.* (2012)
I08T_30.14	Campanian Ignimbrite	Y-5	39.85 ± 0.14	$^{40}Ar/^{39}Ar$	Giaccio *et al.* (2017)
I08T_31.93	Pantelleria Green Tuff	Y-6	45.7 ± 1.00	$^{40}Ar/^{39}Ar$	Scaillet *et al.* (2013)

[1]^{14}C are uncalibrated.

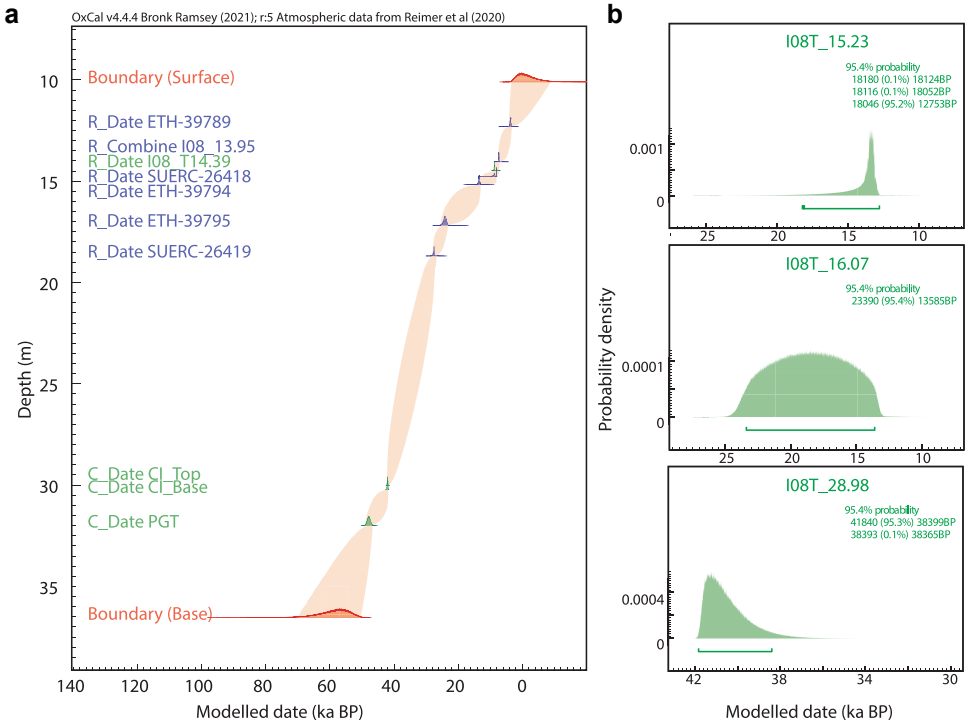

Figure 10. The new I-08 age-depth model, showing: (a) OxCal P_sequence depositional model depth plot, incorporating radiocarbon (blue) and tephra (green) dates, and (b) posterior probability density functions for I08T_16.07 and I08T_15.23. Interpolation and posterior probability density functions are shown at 95.4% confidence limits. [Color figure can be viewed at wileyonlinelibrary.com]

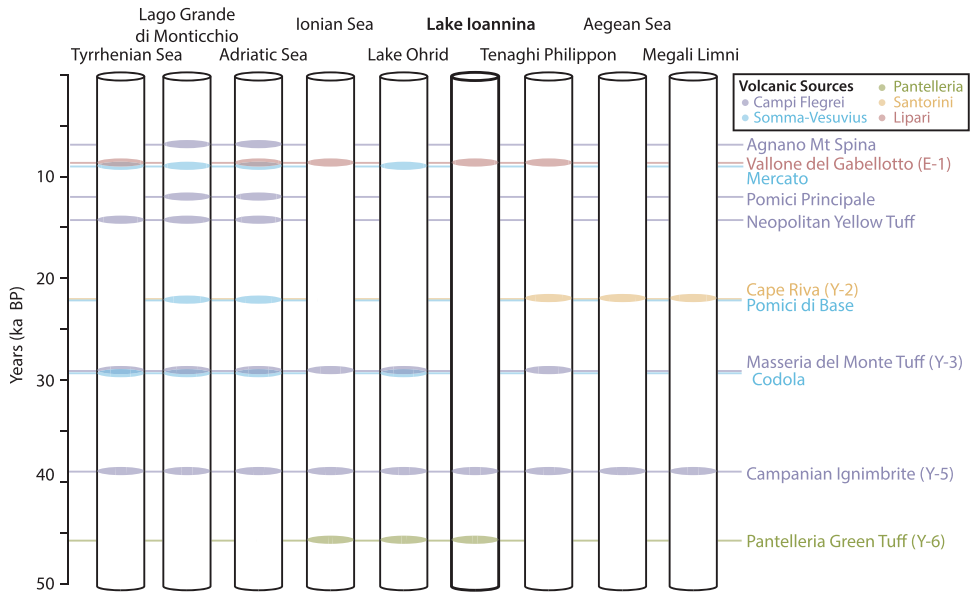

Figure 11. Simplified summary diagram of key tephra horizons within the Mediterranean tephrostratigraphic framework for the past 50 ka. Archives included here are: Tyrrhenian Sea (Paterne *et al.*, 1988; Albert *et al.*, 2012), Lago Grande di Monticchio (Wulf *et al.*, 2004, 2008), Adriatic Sea (Bourne *et al.*, 2010; Matthews *et al.*, 2015), Ionian Sea (Keller *et al.*, 1978; Albert *et al.*, 2012; Insinga *et al.*, 2014), Lake Ohrid (Wagner *et al.*, 2008; Vogel *et al.*, 2010; Sulpizio *et al.*, 2010; Leicher *et al.*, 2016), Lake Ioannina (this study), Tenaghi Philippon (Wulf *et al.*, 2018), the Aegean Sea (Satow *et al.*, 2015), and Megali Limni (Margari *et al.*, 2007). Eruption ages from Bronk Ramsey *et al.* (2015) other than Agnano Mt Spina (Smith *et al.*, 2011), Vallone del Gabellotto (E-1) (Albert *et al.*, 2019), Mercato (Santacroce *et al.*, 2008) and Pantelleria Green Tuff (Y-6) (Scaillet *et al.*, 2013). Site locations are shown in Fig. 1. [Color figure can be viewed at wileyonlinelibrary.com]

in inter-site comparisons of the impact of Heinrich stadial 4 (HS4; 40.2–38.3 ka BP, *sensu.* Sanchez Goñi & Harrison, 2010). High resolution analysis of the I-08 vegetation record in sediments surrounding the I08T_30.14 tephra marker would allow the pattern and timing of the ecosystem response to HS4 at the site to be precisely evaluated and compared to other sites in the eastern Mediterranean.

The ca. 46 ka BP PGT/Y-6 tephra marker facilitates direct correlation to terrestrial records with palaeoenvironmental sequences including Lake Ohrid, and to marine cores from the Sicily channel (Tamburrino *et al.*, 2012) and Ionian Sea (Keller *et al.*, 1978). Together the PGT/Y-6 and CI/Y-5 tephra layers bracket an interval of ca. 6 ka in the Ioannina, Lake Ohrid and Ionian Sea records associated with four Dansgaard-Oeschger events observed in the Greenland ice-core records (Rasmussen *et al.*, 2014). Comparison of palaeoenvironmental proxies within these archives could allow both local to regional and proxy-specific responses to these climate oscillations to be explored with high precision.

The presence of the Campanian Ignimbrite and Pantelleria Green Tuff tephra layers also provides an exciting opportunity to link the valuable palaeoenvironmental record contained within the Ioannina sequence to regional archaeological sites. For example, CI/Y-5 deposits have been identified in the Klissoura and Franchthi sequences (Lowe *et al.*, 2012), and the PGT/Y-6 marker has been identified at Theopetra (Karkanas *et al.*, 2014). These tephra linkages establish a chronological framework which, going forward, we hope will facilitate more thorough investigation of the environmental niches occupied by early Europeans in the region following their expansion out of Africa.

The identification of three cryptotephra layers correlated to Lipari between ca. 16 and 14 m depth in the I-08 sequence provides the first securely dated evidence that Lipari erupted at least three times during the LGIT and Early Holocene. The Vallone del Gabellotto (E-1) isochron connects the Ioannina sequence to archives in the Ionian, Adriatic and Tyrrhenian seas (Albert *et al.*, 2017), and the terrestrial Tenaghi Philippon peat sequence (Wulf *et al.*, 2018). Preliminary dates for the two earlier Lipari cryptotephra layers suggests two more tie points may exist between Ioannina and the Ionian Sea, however, further geochemical data is needed to confirm these findings.

Challenges in cryptotephra analysis of the I-08 core

The frequency of tephra dispersal from explosive eruptions in the Mediterranean region during the last glacial period and the geographical location of Lake Ioannina down-wind from the productive Italian Arc volcanoes, suggested that many cryptotephra layers would be found in the I-08 core sediments. However, cryptotephra analyses did not identify horizons of primary ash fall in the section of the I-08 core between 29 and 18 m.

The identification of discrete tephra layers from Lipari in the Late Glacial and Early Holocene sediments at Ioannina highlight the suitability of the Lake Ioannina sequence for capturing cryptotephra layers. However, during the last glacial when high concentrations of tephra were deposited in the Ioannina catchment from the voluminous Campanian Ignimbrite eruption, the swamping effect of the reworked CI/Y-5 tephra through processes of intra-basin focussing and redistribution of tephra glass shards made the detection of cryptotephra from primary air-fall impossible. Thus, even if primary air-fall tephra layers were present in the I-08 core sequence as cryptotephra horizons they would be difficult to identify against the background of reworked tephra. The challenges associated with identifying primary airfall from closely-spaced eruptions of similar geochemical composition is not a new one in tephrostratigraphic research (e.g. Pyne-O'Donnell *et al.*, 2008). In an attempt to overcome these challenges glass shard colour, grain size, and morphology were carefully considered during microscopic analysis of samples with the aim of detecting any changes in glass shard characteristics that might indicate input of tephra from different sources (McLean *et al.*, 2018). However, as has been

noted from many distal tephra archives, silicic tephra from Mediterranean sources have quite similar morphologies, so few eruptions are distinguishable on the basis of morphology alone (Bourne *et al.*, 2010; Matthews *et al.*, 2015). Thus, it is possible that cryptotephra layers were not found during this study because the shards from different eruptions in the Mediterranean tend to be of similar morphology and colour.

Unexpectedly, this study has demonstrated that the identification of reworked tephra horizons can, in supplement to other proxy data such as grain size and geochemistry, provide an insight into changing processes of erosion, sediment in-wash, and reworking within a lake catchment. The value of detailed sedimentary analyses to understand tephra taphonomy has been demonstrated in this study through the combination of grain size analysis, XRF data, and tephra shard counting. Complex processes of sediment remobilisation and reworking were identified, raising questions about the integrity of the sediment record between 29 and 28.5 m depth as a primary, undisturbed, deposit. The presence of non-contemporaneous tephra within younger sediments suggests in-wash and redeposition of older material from the edge of the lake further into the lake. Determining the age offset between the age of the redeposited material and contemporaneous sedimentation would be a challenge, further highlighting the importance of sediment taphonomy in Quaternary reconstructions.

The absence of tephra evidence for a number of widespread Quaternary eruptions in the I-08 sequence may be due to preferential deposition of tephra deposits near inflows and internal redistribution through currents (Pyne-O'Donnell *et al.*, 2008). For example, internal processes can result in tephra deposits being reworked to below detection levels in some areas of the lake, however, such processes are complex and dynamic (Dugmore & Newton, 2012; Watson *et al.*, 2016). Spatial variation in intra-basin focussing of tephra over time may explain why cryptotephra are present within the sequence over the Late Glacial and Early Holocene but not during other periods.

Methodological recommendations

Syn-depositional and post-depositional tephra transportation have been demonstrated in a range of studies undertaken in lake environments, often revealing large intra-basin variability in visible and/or crypto- tephra layer thickness (Mangerud *et al.*, 1984). In the case of the Ioannina record, where tephrostratigraphic analysis was carried out only on a single core containing evidence of reworked sediment, the record of tephra deposited at lake site may not have been fully captured (Watson *et al.*, 2016). Thus, replication of this study on future cores from the site may provide a more complete picture of tephra deposition at Ioannina.

The omission of key regional tephra markers (e.g. the Y-3) may be a result of small gaps between the core segments, an artefact of the coring methodology applied. Gaps in the stratigraphy mean it is possible that key isochrons may be missing (Lowe, 2011). Furthermore, gaps in the core complicate the identification of the primary ash fall layer and may results in a reworked layer being identified as a primary air-fall deposit, which can result in age attribution of an eruption age to an incorrect depth. Detailed stratigraphic analysis, facilitating the identification of horizons where reworking is likely, can help in developing a robust tephrochronology. We, therefore, highlight the importance of taking overlapping, parallel cores wherever possible, which minimise gaps in the stratigraphy.

Conclusions

The development of an extended independent chronology for the I-08 core is a step forward in the dating of an important palaeoenvironmental record. The integration of the Ioannina site into the Mediterranean tephra framework provides direct correlations with a range of Quaternary sequences in the Mediterranean region. The potential of tephra studies at Ioannina is by no means limited to the last glacial cycle, and tephrochronologies provide opportunities for dating and correlation of records over multiple glacial cycles. Importantly, tephra studies may act as independent checks of earlier, tuned chronologies for Ioannina sequences.

The chronology developed here also opens up opportunities for future work on the I-08 core, particularly the potential for increased resolution, sub-millennial scale study of the proxy record contained within the sediments. Pollen analysis of Ioannina core I-284 has revealed marked vegetation responses to millennial-scale climatic oscillations (Tzedakis *et al.*, 2004). The three secure isochrons, the last glacial Campanian Ignimbrite (CI/Y-5; ca. 39.8 ka BP) and Pantelleria Green Tuff (PGT/Y-6; ca. 45.7 ka BP) and the Holocene Vallone del Gabellotto cryptotephra marker (E-1; ca. 8.3 ka BP) identified in the Ioannina sequence provide opportunities for direct correlation of this pollen record with palaeoenvironmental, palaeoclimate, and archaeological sequences throughout the eastern Mediterranean. In particular, the CI/Y-5 marker provides an opportunity to undertake detailed inter-site comparisons of the timing of ecosystem responses to Heinrich stadial 4 (40.1–28.3 ka BP *sensu.* Sanchez Goñi & Harrison, 2010).

We have highlighted a significant challenge in Mediterranean tephra studies and, indeed, tephra studies globally, which is the identification of primary airfall cryptotephra layers against a background of sediment (and therefore tephra) reworking, particularly in areas where multiple eruptions produce huge volumes of glass shards with similar morphologies and geochemical signatures. In this work, whilst it is possible that the record contains distal deposits from multiple eruptions from Campi Flegrei, particularly those following the Campanian Ignimbrite eruption, it has not been possible to produce reliable correlations through geochemical analysis. The main barrier preventing geochemical attribution of these deposits to subsequent eruptions is the broad geochemical envelope of the large Campanian Ignimbrite eruption which has multiple phases (Tomlinson *et al.*, 2012), many of which are identified at Ioannina. Refining and developing techniques which allow for the further discrimination of these different eruptions will be a crucial step in developing and expanding the Mediterranean tephra chronostratigraphic framework.

Acknowledgements. We thank Tim Jones and Vicky Cullen for supporting the work on the Holocene and Lateglacial sections of the core. We are also indebted to Chronis Tzedakis and Ian Lawson for providing the I-08 core and numerous constructive comments on the manuscript, and to Harriet Allen for her support throughout this project. Iris Buisman and Victoria Smith kindly supported EPMA analysis. AMM was funded by a PhD studentship from the Department of Geography, University of Cambridge. Initial work by CSL and PGA was supported via the NERC-funded project Response of Humans to Abrupt Environmental Transitions (RESET; NE/E015670/1). RK was supported by the NERC-funded Environmental Research Doctoral Training Program (NE/L002613/1) at the University of Oxford. We thank Sabine Wulf, Roberto Sulpizio, and Simon Blockley for their constructive feedback on the manuscript.

Data availability statement

The data that supports the findings of this study are available in the supplementary material of this article.

Supporting information

Additional supporting information can be found in the online version of this article.

Figure S1. Major element geochemistry for tephra glass shards from visible tephra layer I08T_31.93, showing: (a) total alkali vs. silica plot (Le Bas et al., 1986) and (b) FeOt vs AlO3, plotted alongside geochemical data from proximal Pantelleria Green Tuff deposits and distal occurrences of the Y-6 tephra marker.

Figure S2. Particle size distributions for visible tephra layer I08T_30.14, showing upward fining.

Figure S3. Major element geochemistries for tephra glass shards from visible tephra layer I08T_30.14 plotted alongside geochemical data from proximal Campanian Ignimbrite deposits and distal occurrences of the Y-5 tephra marker.

Figure S4. Biplot showing major element glass compositions of cryptotephra I08T_31.17 and I08T_30.74 m, showing the geochemical field of the visible I08T_30.14 tephra marker, and medial-distal products of Campi Flegrei with a stratigraphic position below the CI.

Figure S5. Major element geochemistry of tephra glass shards from I-08 cryptotephra layers between 29.88 and 28.51 m depth, showing glass shard concentrations alongside major and minor element compositions for identified peaks. Plotted for comparison are the major and minor element compositions of selected widespread tephra markers originating from Campi Flegrei including proximal (Tomlinson et al., 2015), and distal correlatives from Ionian Sea core M25/4-12 (Albert et al., 2015), Lago Grande di Monticchio (Wulf et al., 2004) and Tenaghi Philippon (Wulf et al., 2018).

Figure S6. Scatter plot matrix showing the full (wt%) major and minor element geochemical composition of I-08 tephra layers I08T_28.98 and I08T 30.14, in addition to the composition of the Y-3 tephra marker from the type site in the Ionian Sea (Albert et al., 2015).

Figure S7. Probability density function for the remodelled Caron et al. (2012) age of the Vallone del Gabelloto (VdG/E-1) eruption (with 95.4% highest probability density ranges shown).

References

Albert P, Hardiman M, Keller J *et al*. 2015. Revisiting the Y-3 tephrostratigraphic marker: A new diagnostic glass geochemistry, age estimate, and details on its climatostratigraphical context. *Quaternary Science Reviews* **118**: 105–121.

Albert P, Tomlinson EL, Lane CS *et al*. 2013. Late glacial explosive activity on Mount Etna: Implications for proximal-distal tephra correlations and the synchronisation of Mediterranean archives. *Journal of Volcanology and Geothermal Research* **265**: 9–26.

Albert PG, Giaccio B, Isaia R *et al*. 2019. Evidence for a large-magnitude eruption from Campi Flegrei caldera (Italy) at 29 ka. *Geology* **47**(7): 595–599.

Albert PG, Tomlinson EL, Smith VC *et al*. 2012. Marine-continental tephra correlations: Volcanic glass geochemistry from the Marsili Basin and the Aeolian Islands, Southern Tyrrhenian Sea, Italy. *Journal of Volcanology and Geothermal Research* **229-230**: 74–94.

Albert PG, Tomlinson EL, Smith VC *et al*. 2017. Glass geochemistry of pyroclastic deposits from the Aeolian Islands in the last 50 ka: A proximal database for tephrochronology. *Journal of Volcanology and Geothermal Research* **336**: 81–107.

Allen JRL, Huntley B, Brandt U *et al*. 1999. Rapid environmental changes in southern Europe during the last glacial period. *Nature* **400**(6746): 740–743.

Andersen KK, Azuma N, Barnola JM *et al*. 2004. High-resolution record of Northern Hemisphere climate extending into the last interglacial period. *Nature* **431**(7005): 147–151.

Blaauw M. 2012. Out of tune: The dangers of aligning proxy archives. *Quaternary Science Reviews* **36**: 38–49.

Blaauw M, Christen JA, Bennett K *et al*. 2018. Double the dates and go for Bayes—Impacts of model choice, dating density and quality on chronologies. *Quaternary Science Reviews* **188**: 58–66.

Blockley SP, Bourne AJ, Brauer A *et al*. 2014. Tephrochronology and the extended intimate (integration of ice-core, marine and terrestrial records) event stratigraphy 8-128 ka b2k. *Quaternary Science Reviews* **106**: 88–100.

Blockley SP, Pyne-O'Donnell S, Lowe J *et al*. 2005. A new and less destructive laboratory procedure for the physical separation of distal glass tephra shards from sediments. *Quaternary Science Reviews* **24**(16): 1952–1960.

Bond G, Broecker W, Johnsen S *et al*. 1993. Correlations between climate records from North Atlantic sediments and Greenland ice. *Nature* **365**(6442): 143–147.

Bourne A, Albert P, Matthews I *et al*. 2015. Tephrochronology of core prad 1-2 from the Adriatic sea: Insights into Italian explosive volcanism for the period 200-80 ka. *Quaternary Science Reviews* **116**: 28–43.

Bourne AJ, Lowe J, Trincardi F *et al*. 2010. Distal tephra record for the last ca 105,000 years from core PRAD 1-2 in the central Adriatic Sea: Implications for marine tephrostratigraphy. *Quaternary Science Reviews* **29**(23–24): 3079–3094.

Bronk Ramsey C. 2009. Bayesian analysis of radiocarbon dates. *Radiocarbon* **51**(1): 337–360.

Bronk Ramsey C. 2020. OxCal v4.4. https://c14.arch.ox.ac.uk/OxCal/OxCal.html

Bronk Ramsey C, Albert P, Blockley SP *et al*. 2015. Improved age estimates for key Late Quaternary European tephra horizons in the RESET lattice. *Quaternary Science Reviews* **118**: 18–32.

Buckland HM, Cashman KV, Engwell SL *et al*. 2020. Sources of uncertainty in the Mazama isopachs and the implications for interpreting distal tephra deposits from large magnitude eruptions. *Bulletin of Volcanology* **82**(3): 1–17.

Caron B, Siani G, Sulpizio R *et al*. 2012. Late Pleistocene to Holocene tephrostratigraphic record from the Northern Ionian Sea. *Marine Geology* **311–314**: 41–51.

Civetta L, Cornette Y, Crisci G *et al*. 1984. Geology, geochronology and chemical evolution of the island of Pantelleria. *Geological Magazine* **121**(6): 541–562.

Conispoliatis N, Panagos A, Perissoratis C, Varnavas S. 1986. Geological and sedimentological patterns in the lake Pamvotis (Ioannina), N. W. Greece. *Annales Géologiques des Pays Helléniques* **33**(1): 269–286.

Costa A, Folch A, Macedonio G *et al*. 2012. Quantifying volcanic ash dispersal and impact of the Campanian Ignimbrite super-eruption. *Geophysical Research Letters* **39**(10): 1–16.

Cullen VL, Smith VC, Arz HW. 2014. The detailed tephrostratigraphy of a core from the south-east Black Sea spanning the last ~60 ka. *Journal of Quaternary Science* **29**(7): 675–690.

Dansgaard W, Clausen HB, Gundestrup N *et al*. 1982. A new Greenland deep ice core. *Science* **218**(4579): 1273–1277.

Dansgaard W, Johnsen SJ, Clausen HB *et al*. 1993. Evidence for general instability of past climate from a 250-kyr ice-core record. *Nature* **364**(6434): 218–220.

Davies S. 2015. Cryptotephras: The revolution in correlation and precision dating. *Journal of Quaternary Science* **30**(2): 114–130.

Dominguez L, Bonadonna C, Forte P *et al*. 2020. Aeolian remobilisation of the 2011-Cordón Caulle Tephra-Fallout deposit: Example of an important process in the life cycle of volcanic ash. *Frontiers in Earth Science* **7**: 343.

Dugmore A, Newton A. 2012. Isochrons and beyond: Maximising the use of tephrochronology in geomorphology. *Jökull* **62**: 39–52.

Eastwood W, Pearce N, Westgate J *et al*. 1999. Geochemistry of Santorini tephra in lake sediments from Southwest Turkey. *Global and Planetary Change* **21**(1-3): 17–29.

Engwell SL, Sparks RS, Carey S. 2014. Physical characteristics of tephra layers in the deep sea realm: The Campanian Ignimbrite eruption. *Geological Society Special Publication* **398**(1): 47–64.

Fitzsimmons KE, Hambach U, Veres D *et al*. 2013. The Campanian Ignimbrite eruption: New data on volcanic ash dispersal and its potential impact on human evolution. *PLoS ONE* **8**(6): e65839.

Frogley MR, Griffiths HI, Heaton THE. 2009. Historical biogeography and Late Quaternary environmental change of Lake Pamvotis,

Ioannina (north-western Greece): Evidence from ostracods. *Journal of Biogeography* **28**(6): 745–756.

Gehrels MJ, Lowe DJ, Hazell ZJ *et al*. 2006. A continuous 5300-yr Holocene cryptotephrostratigraphic record from northern New Zealand and implications for tephrochronology and volcanic hazard assessment. *The Holocene* **16**(2): 173–187.

Giaccio B, Hajdas I, Isaia R *et al*. 2017. High-precision ^{14}C and 40Ar/39Ar dating of the Campanian Ignimbrite (Y-5) reconciles the time-scales of climatic-cultural processes at 40 ka. *Scientific Reports* **7**(1): 45940.

Goñi MFS, Turon J-L, Eynaud F *et al*. 2000. European climatic response to millennial-scale changes in the atmosphere-ocean system during the last glacial period. *Quaternary Research* **54**(3): 394–403.

Hardiman MJ. 2012. *Testing and refining the chronology and correlation of Mediterranean pollen records of late Last Glacial age using tephrochronology*. PhD thesis, University of London, Royal Holloway.

Hayward C. 2012. High spatial resolution electron probe microanalysis of tephras and melt inclusions without beam-induced chemical modification. *The Holocene* **22**: 119–125.

Higgs ES, Vita-Finzi C, Harris DR *et al*. 1967. The climate, environment and industries of Stone Age Greece: Part III. With an appendix on a late Quaternary pollen diagram from Ioanninae. *Proceedings of the Prehistoric Society* **1**: 199–244.

Insinga DD, Tamburrino S, Lirer F *et al*. 2014. Tephrochronology of the astronomically-tuned KC01B deep-sea core, Ionian Sea: Insights into the explosive activity of the Central Mediterranean area during the last 200ka. *Quaternary Science Reviews* **85**: 63–84.

Jochum KP, Willbold M. 2006. Reference materials in geoanalytical research—Review for 2004 and 2005. *Geostandards and Geoanalytical Research* **30**(3): 143–156.

Johnsen SJ, Clausen HB, Dansgaard W *et al*. 1992. Irregular glacial interstadials recorded in a new Greenland ice core. *Nature* **359**(6393): 311–313.

Jones TD, Lawson IT, Reed JM *et al*. 2013. Diatom-inferred late Pleistocene and Holocene palaeolimnological changes in the Ioannina basin, northwest Greece. *Journal of Paleolimnology* **49**(2): 185–204.

Jordan NJ, Rotolo SG, Williams R *et al*. 2018. Explosive eruptive history of Pantelleria, Italy: Repeated caldera collapse and ignimbrite emplacement at a peralkaline volcano. *Journal of Volcanology and Geothermal Research* **349**: 47–73.

Karkanas P, White D, Lane CS *et al*. 2014. Tephra correlations and climatic events between the MIS6/5 transition and the beginning of MIS3 in Theopetra Cave, central Greece. *Quaternary Science Reviews* **118**: 170–181.

Keller J, Ryan WB, Ninkovich D *et al*. 1978. Explosive volcanic activity in the Mediterranean over the past 200,000 yr as recorded in deep-sea sediments. *Bulletin of The Geological Society of America* **89**(4): 591–604.

Lane CS, Chorn BT, Johnson TC. 2013. Ash from the Toba supereruption in Lake Malawi shows no volcanic winter in East Africa at 75 ka. *Proceedings of the National Academy of Sciences of The United States of America* **110**(20): 8025–8029.

Lane CS, Cullen V, White D *et al*. 2014. Cryptotephra as a dating and correlation tool in archaeology. *Journal of Archaeological Science* **42**(1): 42–50.

Lawson IT. 2001. *The Late Glacial and Holocene environmental history of Greece*. PhD thesis, University of Cambridge.

Lawson IT, Frogley M, Bryant CL *et al*. 2004. The Lateglacial and Holocene environmental history of the Ioannina basin, north-west Greece. *Quaternary Science Reviews* **23**(14): 1599–1625.

Le Bas MJ, Maitre RW, Streckeisen A *et al*. 1986. A chemical classification of volcanic rocks based on the total alkali-silica diagram. *Journal of Petrology* **27**(3): 745–750.

Leicher N, Zanchetta G, Sulpizio R *et al*. 2016. First tephrostratigraphic results of the DEEP site record from Lake Ohrid (Macedonia and Albania). *Biogeosciences* **13**: 2151–2178.

Li C, Born A. 2019. Coupled atmosphere-ice-ocean dynamics in Dansgaard-Oeschger events. *Quaternary Science Reviews* **203**: 1–20.

Lowe DJ. 2011. Tephrochronology and its application: A review. *Quaternary Geochronology* **6**(2): 107–153.

Lowe J, Barton N, Blockley SP *et al*. 2012. Volcanic ash layers illuminate the resilience of Neanderthals and early modern humans to natural hazards. *Proceedings of the National Academy of Sciences* **109**(34): 13532–7.

Lowe J, Rasmussen S, Björck S *et al*. 2008. Synchronisation of palaeoenvironmental events in the north Atlantic region during the last termination: A revised protocol recommended by the INTIMATE group. *Quaternary Science Reviews* **27**(1): 6–17. INTegration of Ice-core, Marine and Terrestrial records (INTIMATE): Refining the record of the Last Glacial-Interglacial Transition.

Lowe J, Walker MJ. 2015. Measuring quaternary time: A 50-year perspective. *Journal of Quaternary Science* **30**(2): 104–113.

Mahood GA, Hildreth W. 1986. Geology of the peralkaline volcano at Pantelleria, Strait of Sicily. *Bulletin of Volcanology* **48**(2-3): 143–172.

Mangerud JaN, Lie E, Furnes H *et al*. 1984. A Younger Dryas Ash Bed in western Norway, and its possible correlations with tephra in cores from the Norwegian Sea and the North Atlantic. *Quaternary Research* **104**: 85–104.

Margari V, Pyle D, Bryant CL *et al*. 2007. Mediterranean tephra stratigraphy revisited: Results from a long terrestrial sequence on Lesvos Island, Greece. *Journal of Volcanology and Geothermal Research* **163**(1): 34–54.

Marra F, Castellano C, Cucci L *et al*. 2020. Monti Sabatini and Colli Albani: The dormant twin volcanoes at the gates of Rome. *Scientific Reports* **10**(1): 8666.

Matthews IP, Trincardi F, Lowe JJ *et al*. 2015. Developing a robust tephrochronological framework for Late Quaternary marine records in the Southern Adriatic Sea: New data from core station SA03-11. *Quaternary Science Reviews* **118**: 84–104.

McLean D, Albert PG, Nakagawa T *et al*. 2018. Integrating the Holocene tephrostratigraphy for East Asia using a high-resolution cryptotephra study from Lake Suigetsu (SG14 core), central Japan. *Quaternary Science Reviews* **183**: 36–58.

Melekestsev IV, Kirianov V, Praslov ND. 1984. Catastrophic eruption in the Phlegrean Fields region (Italy)—Possible source for a volcanic ash in late Pleistocene sediments on the European part of the USSR. *Vulcanologija i Seismologija* **3**: 35–44.

Menviel LC, Skinner LC, Tarasov L *et al*. 2020. An ice-climate oscillatory framework for Dansgaard-Oeschger cycles. *Nature Reviews Earth & Environment* **1**(12): 677–693.

Morley MW, Woodward JC. 2011. The Campanian Ignimbrite (Y5) tephra at Crvena Stijena Rockshelter, Montenegro. *Quaternary Research* **75**(3): 683–696.

Müller UC, Pross J, Tzedakis PC *et al*. 2011. The role of climate in the spread of modern humans into Europe. *Quaternary Science Reviews* **30**(3-4): 273–279.

Negri A, Capotondi L, Keller J. 1999. Calcareous nannofossils, planktonic foraminifera and oxygen isotopes in the late Quaternary sapropels of the Ionian Sea. *Marine Geology* **157**(1–2): 89–103.

Neugebauer I, Wulf S, Schwab MJ *et al*. 2017. Implications of s1 tephra findings in Dead Sea and Tayma palaeolake sediments for marine reservoir age estimation and palaeoclimate synchronisation. *Quaternary Science Reviews* **170**: 269–275.

Pappalardo L, Civetta L, D'Antonio M *et al*. 1999. Chemical and Sr-isotopical evolution of the Phlegraean magmatic system before the Campanian Ignimbrite and the Neapolitan Yellow Tuff eruptions. *Journal of Volcanology and Geothermal Research* **91**(2–4): 141–166.

Paterne M, Guichard F, Duplessy JC *et al*. 2008. A 90,000-200,000 yrs marine tephra record of Italian volcanic activity in the Central Mediterranean Sea. *Journal of Volcanology and Geothermal Research* **177**(1): 187–196.

Paterne M, Guichard F, Labeyrie J. 1988. Explosive activity of the South Italian volcanoes during the past 80,000 years as determined by marine tephrochronology. *Journal of Volcanology and Geothermal Research* **34**(3-4): 153–172.

Peretyazhko IS, Savina EA, Karmanov NS *et al*. 2015. Genesis of mugearites and benmoreites of Nemrut volcano, eastern Turkey: Magma mixing and fractional crystallization of trachybasaltic melt. *Petrology* **23**(4): 376–403.

Pyle DM, Ricketts GD, Margari V *et al*. 2006. Wide dispersal and deposition of distal tephra during the Pleistocene 'Campanian

Ignimbrite/Y5′ eruption, Italy. *Quaternary Science Reviews* **25**(21–22): 2713–2728.
Pyne-O'Donnell S, Blockley S, Turney C *et al*. 2008. Distal volcanic ash layers in the Lateglacial Interstadial (gi-1): Problems of stratigraphic discrimination. *Quaternary Science Reviews* **27**(1): 72–84. INTegration of Ice-core, Marine and Terrestrial records (INTIMATE): Refining the record of the Last Glacial-Interglacial Transition.
Ramsey CB. 2008. Deposition models for chronological records. *Quaternary Science Reviews* **27**(1–2): 42–60.
Ramsey CB, Lee S. 2013. Recent and planned developments of the program OxCal. *Radiocarbon* **55**(2–3): 720–730.
Rasmussen SO, Bigler M, Blockley SP *et al*. 2014. A stratigraphic framework for abrupt climatic changes during the Last Glacial period based on three synchronized Greenland ice-core records: Refining and extending the INTIMATE event stratigraphy. *Quaternary Science Reviews* **106**: 14–28.
Reimer PJ. 2020. The IntCal20 Northern Hemisphere radiocarbon age calculation curve (0-55 cal kBP). *Radiocarbon* **62**(4): 1–33.
Romero JR, Kagalou I, Imberger J *et al*. 2002. Seasonal water quality of shallow and eutrophic Lake Pamvotis, Greece: Implications for restoration. *Hydrobiologia* **474**(1): 91–105.
Rotolo SG, Scaillet S, La Felice S *et al*. 2013. A revision of the structure and stratigraphy of pre-Green Tuff ignimbrites at Pantelleria (Strait of Sicily). *Journal of Volcanology and Geothermal Research* **250**: 61–74.
Roucoux K, Tzedakis PC, Frogley M *et al*. 2008. Vegetation history of the marine isotope stage 7 interglacial complex at Ioannina, NW Greece. *Quaternary Science Reviews* **27**(13): 1378–1395.
Roucoux KH, Shackleton NJ, De Abreu L *et al*. 2001. Combined marine proxy and pollen analyses reveal rapid Iberian vegetation response to north Atlantic millennial-scale climate oscillations. *Quaternary Research* **56**: 128–132.
Roucoux KH, Tzedakis PC, Lawson IT *et al*. 2011. Vegetation history of the penultimate glacial period (Marine isotope stage 6) at Ioannina, north-west Greece. *Journal of Quaternary Science* **26**(6): 616–626.
Sanchez Goñi MF, Harrison SP. 2010. Millennial-scale climate variability and vegetation changes during the Last Glacial: Concepts and terminology. *Quaternary Science Reviews* **29**(21–22): 2823–2827.
Santacroce R, Cioni R, Marianelli P *et al*. 2008. Age and whole rock-glass compositions of proximal pyroclastics from the major explosive eruptions of Somma-Vesuvius: A review as a tool for distal tephrostratigraphy. *Journal of Volcanology and Geothermal Research* **177**(1): 1–18.
Satow C, Tomlinson EL, Grant KM *et al*. 2015. A new contribution to the Late Quaternary tephrostratigraphy of the Mediterranean: Aegean Sea core LC21. *Quaternary Science Reviews* **117**: 96–112.
Scaillet S, Vita-Scaillet G, Rotolo SG. 2013. Millennial-scale phase relationships between ice-core and Mediterranean marine records: Insights from high-precision 40Ar/39Ar dating of the Green Tuff of Pantelleria, Sicily Strait. *Quaternary Science Reviews* **78**: 141–154.
Shotton FW. 1972. An example of hard-water error in radiocarbon dating of vegetable matter. *Nature* **240**(5382): 460–461.
Siani G, Sulpizio R, Paterne M *et al*. 2004. Tephrostratigraphy study for the last 18,000 ^{14}C years in a deep-sea sediment sequence for the South Adriatic. *Quaternary Science Reviews* **23**(23): 2485–2500.
Smith VC, Isaia R, Pearce NJ. 2011. Tephrostratigraphy and glass compositions of post-15 kyr Campi Flegrei eruptions: Implications for eruption history and chronostratigraphic markers. *Quaternary Science Reviews* **30**(25–26): 3638–3660.
Staff RA, Hardiman M, Bronk Ramsey C *et al*. 2019. Reconciling the Greenland ice-core and radiocarbon timescales through the Laschamp geomagnetic excursion. *Earth and Planetary Science Letters* **520**: 1–9.
Sulpizio R, Zanchetta G, Paterne M *et al*. 2003. A review of tephrostratigraphy in central and southern Italy during the last 65 ka. *Alpine and Mediterranean Quaternary* **16**(1): 91–108.
Sulpizio R, Zanchetta G, Vogel H *et al*. 2010. Tephrostratigraphy and tephrochronology of lakes Ohrid and Prespa, Balkans. *Biogeosciences* **7**: 3273–3288.
Sun SS, McDonough WF. 1989. Chemical and isotopic systematics of oceanic basalts: Implications for mantle composition and processes. *Geological Society Special Publication* **42**(1): 313–345.
Tamburrino S, Insinga DD, Sprovieri M *et al*. 2012. Major and trace element characterization of tephra layers offshore Pantelleria Island: Insights into the last 200 ka of volcanic activity and contribution to the Mediterranean tephrochronology. *Journal of Quaternary Science* **27**(2): 129–140.
Tomlinson EL, Arienzo I, Civetta L *et al*. 2012. Geochemistry of the Phlegraean Fields (Italy) proximal sources for major Mediterranean tephras: Implications for the dispersal of Plinian and co-ignimbritic components of explosive eruptions. *Geochimica et Cosmochimica Acta* **93**: 102–128.
Tomlinson EL, Smith VC, Albert P *et al*. 2015. The major and trace element glass compositions of the productive Mediterranean volcanic sources: Tools for correlating distal tephra layers in and around Europe. Quaternary Science Reviews.
Tomlinson EL, Thordarson T, Müller W *et al*. 2010. Microanalysis of tephra by LA-ICP-MS—Strategies, advantages and limitations assessed using the Thorsmörk ignimbrite (Southern Iceland). *Chemical Geology* **279**(3): 73–89.
Tryon CA, Logan MAV, Mouralis D *et al*. 2009. Building a tephrostratigraphic framework for the Paleolithic of Central Anatolia, Turkey. *Journal of Archaeological Science* **36**(3): 637–652.
Tzedakis PC. 1994. Vegetation change through glacial-interglacial cycles: A long pollen sequence perspective. *Philosophical Transactions of the Royal Society B: Biological Sciences* **345**(1314): 403–432.
Tzedakis PC. 2002. Buffered tree population changes in a quaternary refugium: Evolutionary implications. *Science* **297**(5589): 2044–2047.
Tzedakis PC, Frogley M, Lawson IT *et al*. 2004. Ecological thresholds and patterns of millennial-scale climate variability: The response of vegetation in Greece during the last glacial period. *Geology* **32**(2): 109–112.
van der Bilt WG, Lane CS, Bakke J. 2017. Ultra-distal Kamchatkan ash on Arctic Svalbard: Towards hemispheric cryptotephra correlation. *Quaternary Science Reviews* **164**: 230–235.
Vogel H, Wagner B, Zanchetta G *et al*. 2010. A paleoclimate record with tephrochronological age control for the last glacial-interglacial cycle from Lake Ohrid, Albania and Macedonia. *Journal of Paleolimnology* **44**(1): 295–310.
Wagner B, Wulf S, Wessels M *et al*. 2008. The last 40 ka tephrostratigraphic record of Lake Ohrid, Albania and Macedonia: A very distal archive for ash dispersal from Italian volcanoes. *Journal of Volcanology and Geothermal Research* **177**(1): 71–80.
Watson EJ, Swindles GT, Stevenson JA *et al*. 2016. The transport of Icelandic volcanic ash: Insights from northern European cryptotephra records. *Journal of Geophysical Research: Solid Earth* **121**(10): 7177–7192.
Wulf S, Hardiman MJ, Staff RA *et al*. 2018. The marine isotope stage 1–5 cryptotephra record of Tenaghi Philippon, Greece: Towards a detailed tephrostratigraphic framework for the Eastern Mediterranean region. *Quaternary Science Reviews* **186**: 236–262.
Wulf S, Keller J, Satow C *et al*. 2020. Advancing Santorini's tephrostratigraphy: New glass geochemical data and improved marine-terrestrial tephra correlations for the past ~360 kyrs. *Earth-Science Reviews* **200**: 102964.
Wulf S, Kraml M, Brauer A *et al*. 2004. Tephrochronology of the 100 ka lacustrine sediment record of Lago Grande di Monticchio (southern Italy). *Quaternary International* **122**: 7–30.
Wulf S, Kraml M, Keller J. 2008. Towards a detailed distal tephrostratigraphy in the Central Mediterranean: The last 20,000 yrs record of Lago Grande di Monticchio. *Journal of Volcanology and Geothermal Research* **177**(1): 118–132.
Wutke K, Wulf S, Hardiman M *et al*. 2015. Geochemical properties and environmental impacts of seven Campanian tephra layers deposited between 40 and 38 ka BP in the varved lake sediments of Lago Grande di Monticchio, southern Italy. *Quaternary Science Reviews* **118**: 67–83.

